AD-A054 449 ARMY ELECTRONICS RESEARCH AND DEVELOPMENT COMMAND FO--ETC F/G 11/2
TIN OXIDE ROOM TEMPERATURE EMITTER STUDY.(U)
JAN 78 H H KEDESDY, R SARTORE

UNCLASSIFIED DELET-TR-78-4 NL

| OF |
AD
A054449

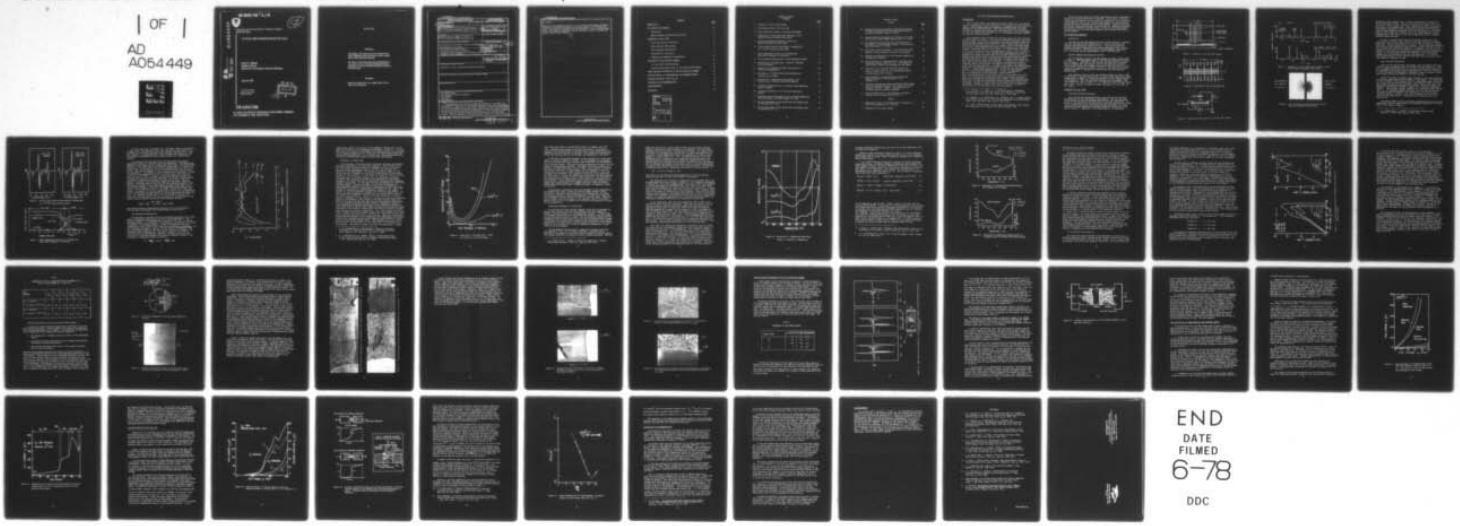

END
DATE
FILMED
6-78
DDC

FOR FURTHER TRAN

AD A054449

AD No.
DDC FILE COPY

RESEARCH AND DEVELOPMENT TECHNICAL REPORT
DELET-TR-78-4

TIN OXIDE ROOM TEMPERATURE EMITTER STUDY

Horst H. Kedesdy
Richard Sartore
Electronics Technology & Devices Laboratory

January 1978

ERADCOM

US ARMY ELECTRONICS RESEARCH & DEVELOPMENT COMMAND
FORT MONMOUTH, NEW JERSEY 07703

NOTICES

Disclaimers

The findings in this report are not to be construed as an official Department of the Army position, unless so designated by other authorized documents.

The citation of trade names and names of manufacturers in this report is not to be construed as official Government indorsement or approval of commercial products or services referenced herein.

Disposition

Destroy this report when it is no longer needed. Do not return it to the originator.

UNCLASSIFIED

SECURITY CLASSIFICATION OF THIS PAGE (When Data Entered)

REPORT DOCUMENTATION PAGE

READ INSTRUCTIONS BEFORE COMPLETING FORM

1. REPORT NUMBER: DELET-TR-78-4
2. GOVT ACCESSION NO.
3. RECIPIENT'S CATALOG NUMBER
4. TITLE (and Subtitle): Tin Oxide Room Temperature Emitter Study.
5. TYPE OF REPORT & PERIOD COVERED: Technical Report.
6. PERFORMING ORG. REPORT NUMBER
7. AUTHOR(s): Horst H. Kedesdy [redacted] Richard Sartore
8. CONTRACT OR GRANT NUMBER(s)
9. PERFORMING ORGANIZATION NAME AND ADDRESS: USA Electronics Technology & Devices Lab. (ERADCOM), Fort Monmouth, N. J. 07703
10. PROGRAM ELEMENT, PROJECT, TASK AREA & WORK UNIT NUMBERS: 1L1 62705AH 94 E3 17
11. CONTROLLING OFFICE NAME AND ADDRESS: Beam, Plasma And Display Division, US Army Electronics Technology and Devices Lab (ERADCOM) ATTN: DELET-B
12. REPORT DATE: Jan 78
13. NUMBER OF PAGES: 43
14. MONITORING AGENCY NAME & ADDRESS (if different from Controlling Office)
15. SECURITY CLASS. (of this report): Unclassified
15a. DECLASSIFICATION/DOWNGRADING SCHEDULE

16. DISTRIBUTION STATEMENT (of this Report)

Approved for public release; distribution unlimited.

17. DISTRIBUTION STATEMENT (of the abstract entered in Block 20, if different from Report)

18. SUPPLEMENTARY NOTES

19. KEY WORDS (Continue on reverse side if necessary and identify by block number)

Tin Dioxide Films
Room Temperature Electron Emission
Cold Cathode
Activation
Field Emission

20. ABSTRACT (Continue on reverse side if necessary and identify by block number)

The mechanisms of activation and electron emission of tin dioxide film room temperature emitters for cold-cathode application have been investigated. The structure, composition and electrical resistivity of vapor deposited films of various thicknesses and antimony doping concentrations have been determined. Activation and electron emission characteristics, as well as seasoning effects of room temperature emitter elements fabricated from such films have been studied. Data and information obtained have been utilized to extend previous

over

DD FORM 1 JAN 73 1473 EDITION OF 1 NOV 65 IS OBSOLETE

UNCLASSIFIED

SECURITY CLASSIFICATION OF THIS PAGE (When Data Entered)

410 698

#20 (Contd)

analysis of the mechanisms involved in the activation and emission processes. Optimization of material parameters and emitter geometry for efficient and stable room temperature emission have been discussed. A new activation method using a laser beam in conjunction with an electrical current to increase the emitter area has been developed.

CONTENTS

CONTENTS (CONTD)
FIGURES

CONTENTS (CONTD)

FIGURES

TABLES

TIN OXIDE ROOM TEMPERATURE EMITTER STUDY

INTRODUCTION

The tin oxide (SnO_2) room temperature emitter (RTE) as a cold-cathode device is potentially of major importance to the general electron tube technology. These cathodes have the advantage of instant start, low power dissipation, and high efficiency. They can also provide new tube capabilities in electron beam semiconductor (EBS) amplifiers, real time samplers in radar and communication systems, and in close-spaced flat-panel cathode ray tubes for display purposes.

Room temperature electron emission from SnO_2 films, was first reported in 1965 by Russian workers.[1] Their results indicated that SnO_2 films, when suitably shaped and activated, exhibited high electron emission densities, and showed great promise as cold-cathodes. They reported that heating the film by an electrical current leads to a rupture in the necked-down region of the film. They interpreted the nature of the emission, as being field emission originating from the film rupture. In a second paper, published in 1971,[2] the Russians reported new experimental results on the activation and emission of SnO_2 RTE. They extended their phenomenological model by assuming that within the emitter gap (film rupture) formed in the activation process, SnO_2 islands exist on the surface of the quartz substrate which provides high electric field conditions when the applied film voltage is sufficiently high to produce field emission. At higher film voltage, however, they infer that the major contribution to the emission is due to secondary electron emission from the edges of the emitter gap bombarded by the field emitted electrons. To support their model, the Russian workers showed that the experimental data obeyed the laws of field and secondary emission. Another model explaining the RTE in SNO_2 was developed by J. L. Mize,[3] of Beta Industries, Inc., in 1972. He postulated that as a consequence of the activation, a semi-cylindrical SnO_2 - SnO heterojunction is thermally formed in the surface of the SnO_2 film. Hot electrons are ejected across this junction whose interface barrier is controlled by the external film voltage. He hypothesized that there must be some field components directed towards the surface which accelerates electrons in that direction and permits them to escape into the vacuum. Attempts to support this junction concept by theoretical considerations or by observation have been unsuccessful.

---

1. M. I. Elinson, A. G. Zhdan, G. A. Kudintseva and M. E. Chugunova, "The Emission of Hot Electrons and the Field Emission of Electrons from Tin Oxide," Rad. Eng. Elec. Phys. 8, pp. 1290, 1965.

2. V. V. Nikulov, G. A. Kudintseva, M. I. Yelinson, and L. A. Konsul Nikova, "The Emission Properties of Cold Cathodes Employing Tin Dioxide (SnO_2) Films," Rad. Eng. Elec. Phys. 17, pp. 1153, 1971.

3. J. L. Mize, "Investigation of Solid State Cold Cathodes," Final Report, Beta Industries, Inc., Contract No. DAAK-72-C-0163, 1972.

The aim of this study is to better understand the basic mechanisms of activation and electron emission of SnO_2 RTE. This study is directed towards the investigation of the electrical properties of SnO_2 thin films as RTE materials, and to also correlate the results with the activation characteristics and emission nature of RTE elements. Electrons and X-ray diffraction, Auger spectroscopy, and microscopy are applied to elucidate the crystal structure of the SnO_2 film, its surface, and compositional depth profile, and the morphology changes in the activated film area of the RTE element.

TIN DIOXIDE FILM MATERIAL

Preparation

The SnO_2 film and RTE samples doped with various amounts of antimony (Sb) were prepared by Beta Industries, Inc., Dayton, Ohio using the chemical vapor deposition technique (CVD). A tin chloride-antimony chloride solution was sprayed on thin quartz substrates which were pre-heated above 500°C. Controlled SnO_2:Sb film thicknesses ranged from 0.1 - 1.0 micron with Sb concentration of 10^{17} - 10^{21} per cm^3.

Emitter Geometry and Electrical Circuit

The film geometry used for the RTE elements are shown schematically in Figure 1. The necked-down region in the film was prepared by a photo-etch technique. Both ends of the film were metalized with a bi-metal such as chromium with gold overlay on which the leads were attached. Linear arrays of five such elements were fabricated from films on 1/2 by 1 inch quartz substrates, as shown in Figure 2. The photo-etch process separates elements by removing the contact metal and film materials between them.

Each element of such an array was activated before its use as a RTE in the vacuum. The electrical circuit of such activated SnO_2 RTE is shown schematically in Figure 3. During the operation of the electron emitter, a voltage(V_F) of 100 - 300 V was applied across the film element. The film current(I_F), which is about 0.1 - 0.2 mA, and the anode voltage (V_A), at about 1000 V, control the emitter current (I_E), which is in the order of 50 - 100 μA.

PROPERTIES OF SnO_2 FILMS

X-ray and Electron Diffraction

The structure and crystalline state of the CVD SnO_2:Sb film were determined from X-ray diffractometer measurements. The line structure of the diffraction pattern indicated that the film was crystalline. In addition, the positions of the diffraction lines were identical with those of the standard SnO_2 powder diffraction pattern published by the Joint Committee on Powder Diffraction Standards (JCPDS No. 5-0467) as can be seen in Figure 4. Comparison of the intensities of the individual

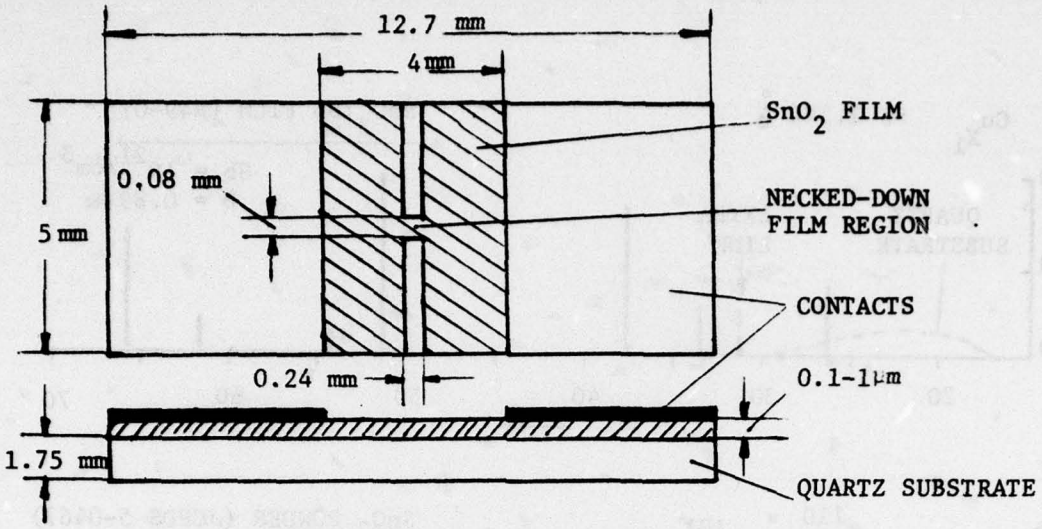

Figure 1. Geometry of the SnO_2 RTE Element

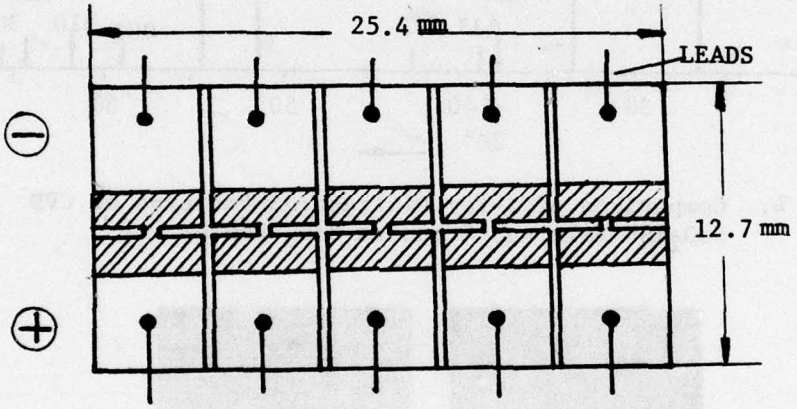

Figure 2. Five-Element Array of the SnO_2 RTE

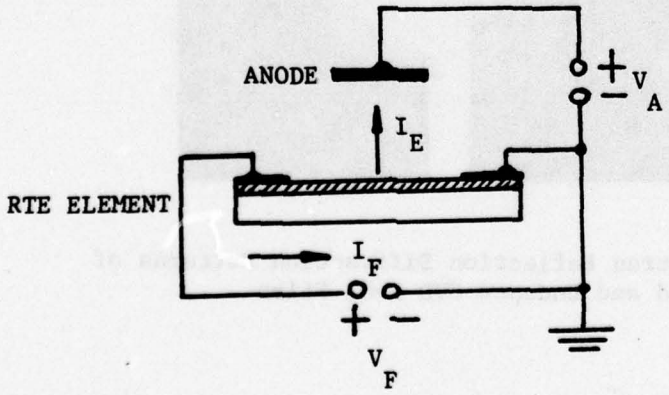

Figure 3. Basic Electrical Circuit of the SnO_2 RTE Element

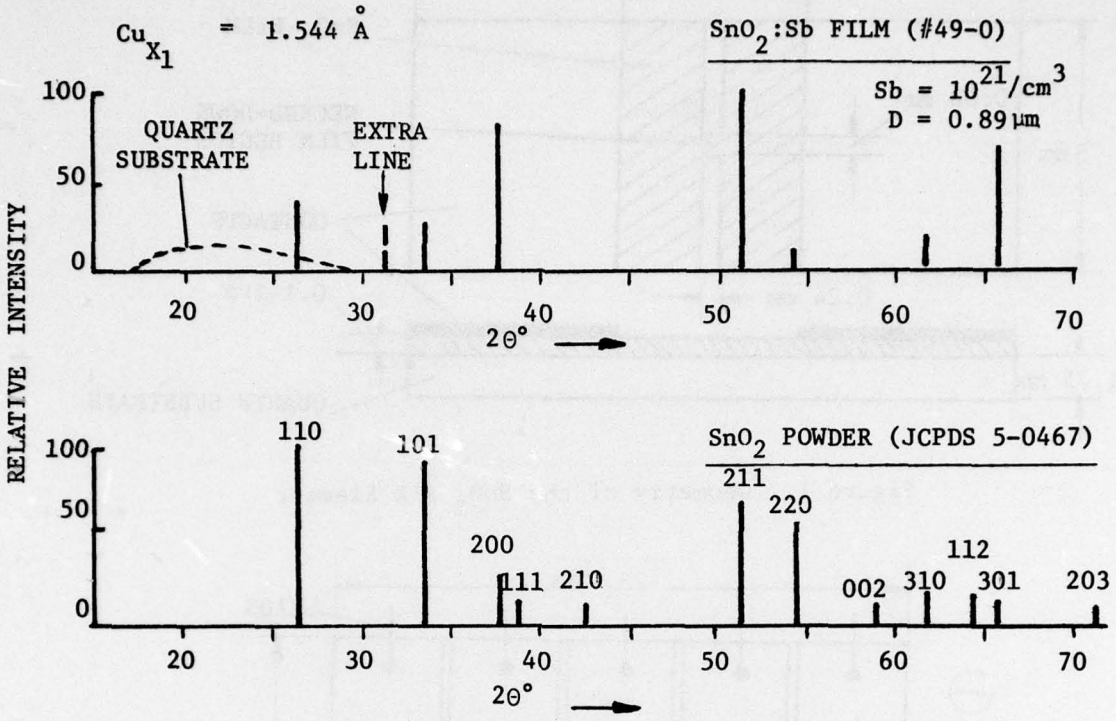

Figure 4. Comparison of X-ray Diffraction Patterns of CVD SnO_2:Sb Film and Standard SnO_2 Powder

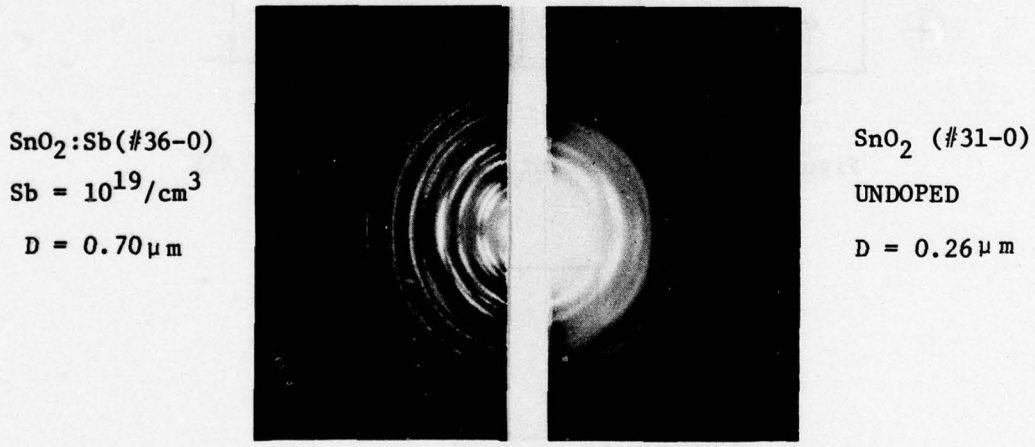

Figure 5. Electron Reflection Diffraction Patterns of Doped and Undoped CVD SnO_2 Films

diffraction lines, however, show distinct differences in intensity of certain diffraction lines. The SnO_2 film diffraction lines at 200, 211, and 301 are much stronger; others are weaker or even absent as compared with those of the standard SnO_2. These differences can be explained by a preferential orientation of the crystallite in the SnO_2 film. The relatively strong intensity enhancement of the 200 diffraction line indicates that the crystallites are oriented with their crystallographic a-axis perpendicular to the surface of the quartz substrate, but are randomly oriented around this axis.

In order to confirm this finding of preferred orientation of the crystallites in CVD SnO_2 films, electron reflection diffraction patterns were taken. The arc-type diffraction ring, as shown in Figure 5, clearly shows that a preferred orientation is evident. It was found that depending on the doping level, different symmetries are observed, as shown for the SnO_2 film with Sb= $10^{19}/cm^3$ and with Sb= 0 (undoped). From this it was concluded that differences in crystallite orientation occur with changing Sb-content. It is also possible that the morphology of the crystallites changes with film thickness during the film deposition. It is known[4] that the growth habit of SnO_2 crystals when grown from a flux melt varies from needles to platelets to rods.

Auger Electron Spectroscopy

Auger electron spectroscopic measurements were performed on CVD SnO_2 films to obtain information about the surface and bulk composition. Since all film samples after deposition on the quartz substrate were exposed to the atmosphere and handled to perform measurements, it was not surprising to find the presence of atmospheric adsorbants, traces of sulphur, carbon, and chlorine from the CVD process on the film surfaces.

Except for carbon, the Auger signal strength for the other adsorbants did not vary appreciably from film sample to film sample. At high amounts of carbon present, it was observed that the constituent oxygen Auger signal at the film surfaces also increased. This indicated that the carbon was probably present as absorbed carbon dioxide. Below the surface, the signals of these impurity elements, except that of chlorine, diminished rapidly. The chlorine, however, remained as an impurity within the bulk film. It is reasonably assumed therefore, that the chlorine has been introduced during the chemical vapor deposition of the film from the chloride solutions. However, it can not be decided if the chlorine is trapped as gas bubbles or is incorporated as an impurity ion in the SnO_2 lattice.

The partial Auger electron spectrogram representing the major tin and oxygen Auger electron energy peaks of an undoped and doped (Sb = $10^{21}/cm^3$) SnO_2 film is shown in Figure 6.

---

4. H. F. Kunkle and E. F. Kohnke, "Flux Growth of Stannic Oxide Crystals," J. Appl. Phys. 36, pp. 1489, 1965.

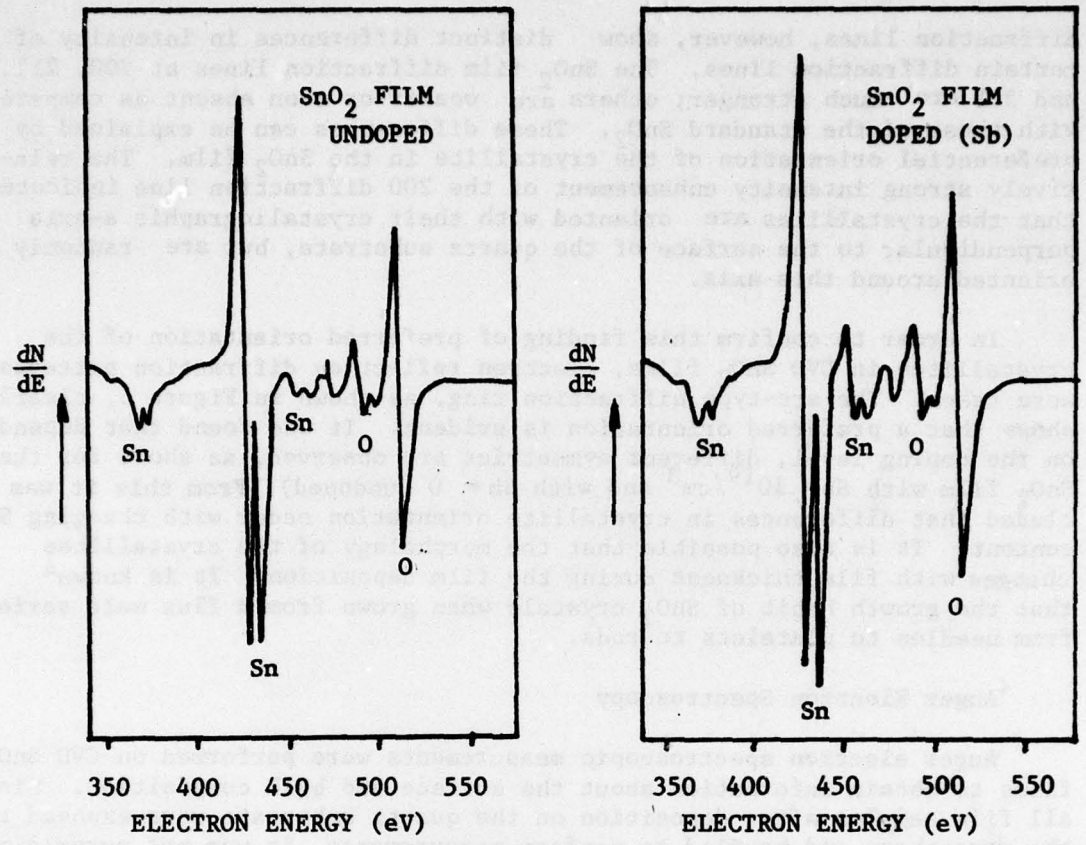

Figure 6. Partial Auger Electron Spectrogram of Undoped and Sb = $10^{21}/cm^3$ Doped CVD SnO_2 Films

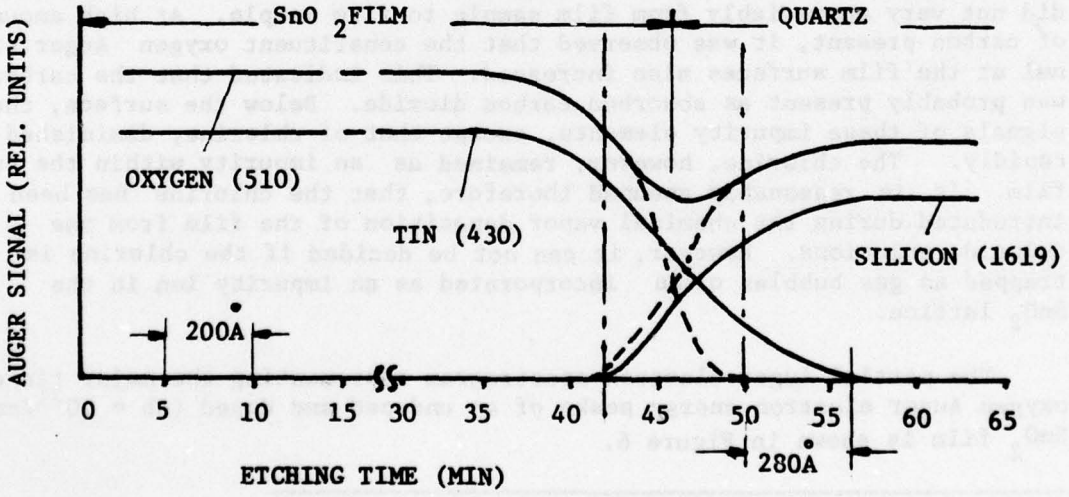

Figure 7. Depth Composition Profile of a Sb-Doped CVD SnO_2 Film, Thickness = 0.18 Micron

It can be seen that the elements tin and oxygen produce a multiplicity of Auger peaks. The spectrum on the right indicates a weak signal of the Sb-dopant at 448 eV which represents the strongest Auger peak of Sb. This peak, however, is overlapping with a small tin peak, and therefore it is not possible to determine its peak-to-peak position for a quantitative analysis.

In conjunction with an argon sputter-etching process, the depth composition profile of a doped SnO_2 film was determined. Multiplexing was employed to only sample the tin, oxygen, and silcon peaks. The peak-to-peak amplitude of the Auger signals was recorded automatically as a function of etching time. The etching of the film was extended down to the quartz substrate. Knowing the thickness of the film and the etching time to reach the substrate, it is possible to relate etching time to film depth. Figure 7 shows the depth composition profile of an 0.18 micron thick SnO_2 film doped with Sb = $10^{21}/cm^3$. Etching is performed completely through the film and partially into the quartz substrate. The profile shows excellent uniformity in composition throughout the depth of the film. After 40 minutes of etching, the silicon Auger signal from the quartz substrate appears, indicating that the SnO_2 film has been completely removed. Upon observation, however, the tin Auger signal continues to decrease as the silicon peak increases. The dip in the oxygen Auger signal shows that the signal is then associated with the constituent oxygen of the SiO_2 substrate. The details of the depth composition profile of the film-substrate interface indicates that small amounts of tin has penetrated the quartz surface. One reasonably assumes that in the first stage of the SnO_2 film deposition, the hydrochloric acid vapor generated by the hydrolysis of the stannic chloride solution on the hot quartz substrate surface:

$$SnCl_4 + 2H_2O \xrightarrow{500 - 800°C} SnO_2 + 4HCl\uparrow$$

had caused etching and consequently diffusion of tin into the surface. From the Auger spectrogram, this diffusion depth is about 600 Å.

Film Thickness Determination

The thickness of the SnO_2 films were determined optically by the transmission interference method using the Cary 14 spectrophotometer. The spectral dependence of transmission was recorded in the 0.3 - 1.6 micron wavelength range. In this region, the variations in transmission are caused principally by interference effects. Figure 8 represents the spectral transmission of $SnO_2 : Sb(10^{17}/cm^3)$ films of three different thicknesses. For film thickness less than 0.1 micron, the high optical transmission causes the interference fringes to fade away and are difficult to measure. For absorption coefficients that are very small compared to the index of refraction and for perpendicular incidence, the basic equation for the calculation of the film thickness from either the maxima or minima of the interference transmission curves is given by:

$$d = \frac{m\lambda max}{2n}, \text{ and } d = \frac{(2m+1)}{4n}\lambda min$$

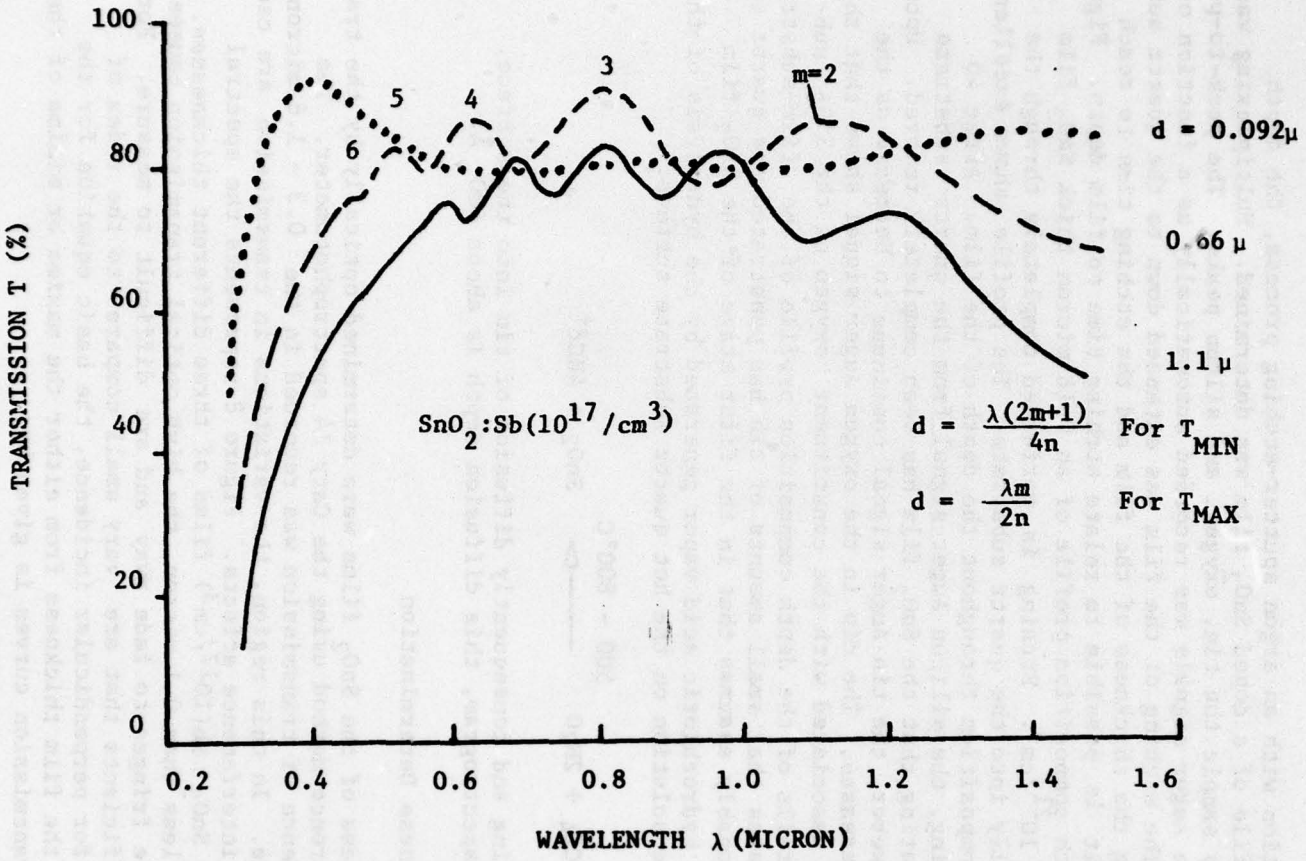

Figure 8. Film Thickness Determination by Interferometric Method

respectively, where m is the order of the maximum or minimum and n is the index of refraction at the corresponding wavelength. Values of n for thin SnO_2 films as a function of wavelength, have been reported in the literature for two antimony doping levels.[5] Values of n for other doping levels were obtained from extrapolation. This non-destructive thickness determination of the SnO_2 films has been found to be quite fast and adequate.

Resistivity of SnO_2 Films

The resistivity of CVD SnO_2 films of different thickness and antimony doping was determined by the four-probe technique. Sets of films on 1/2 by 1 inch quartz substrates ranging in thickness from 0.1 to 1.0 micron and three doping concentrations; Sb =0, $10^{17}/cm^3$, and $10^{21}/cm^3$, were selected for the measurements. The results are shown in Figure 9. The curves show that a desirable low resistivity range exists for thicknesses between 0.2 and 0.4 micron. In this range, the resistivity does not change appreciably with the antimony doping level, and represents a favorable thickness range to achieve reproducible film materials for RTE devices. In general, the curves show that the resistivity decreases with increasing antimony concentration. At very small and large thicknesses the resistivity increases sharply. The sharp increase at very small thicknesses is a known phenomenon observed in thin-film technology and is attributed to an island-type film structure representing a non-continuous film. The strong increase in resistivity at large thicknesses, however, is not common. Usually, as the film thickness increases, its resistivity approaches a constant value which represents the resistivity of a thick pellet or that of the single crystal material. Therefore, one must assume that a chemcial change is responsible for the resistivity increase at large film thicknesses. Since the stoichiometry of the interior of the film does not change with depth as has been found from the Auger electron spectroscopic measurements, it can be reasonably assumed that the presence of chemisorbed oxygen or other atmospheric species are responsible for the increase in resistivity. It has been shown by others[6] that a slight variation in the amount of oxygen chemisorbed on the surface of doped SnO_2 poly-crystalline pellets produces large decreases in electrical conductivity. The n-type conductivity usually found in undoped SnO_2 films provides evidence for lattice defects which give rise to acceptor and donar levels in the band gap. Since the charges associated with these defects are not balanced by self-compensation as evidenced by the n-type character one must assume therefore that an excess of donor levels over the acceptor levels exists. This unbalance gives rise to free electrons which are responsible for the conductivity of the undoped SnO_2 film material. The excess in donors, and hence the conductivity becomes

---

5. S. P. Lyashenko and V. K. Hiloslavskii, "Study of the Optical Properties of Tin Dioxide Thin Films in the Visible and Ultra-Violet Regions," Opt. and Spectr. 19, pp. 55, 1965.

6. H. E. Matthews and E. E. Kohnke, "Effect of Chemisorbed Oxygen on the Electrical Conductivity of Zn-Doped Polycrystalline SnO_2," J. Phys. Chem. Solids, 29, pp. 653, 1968.

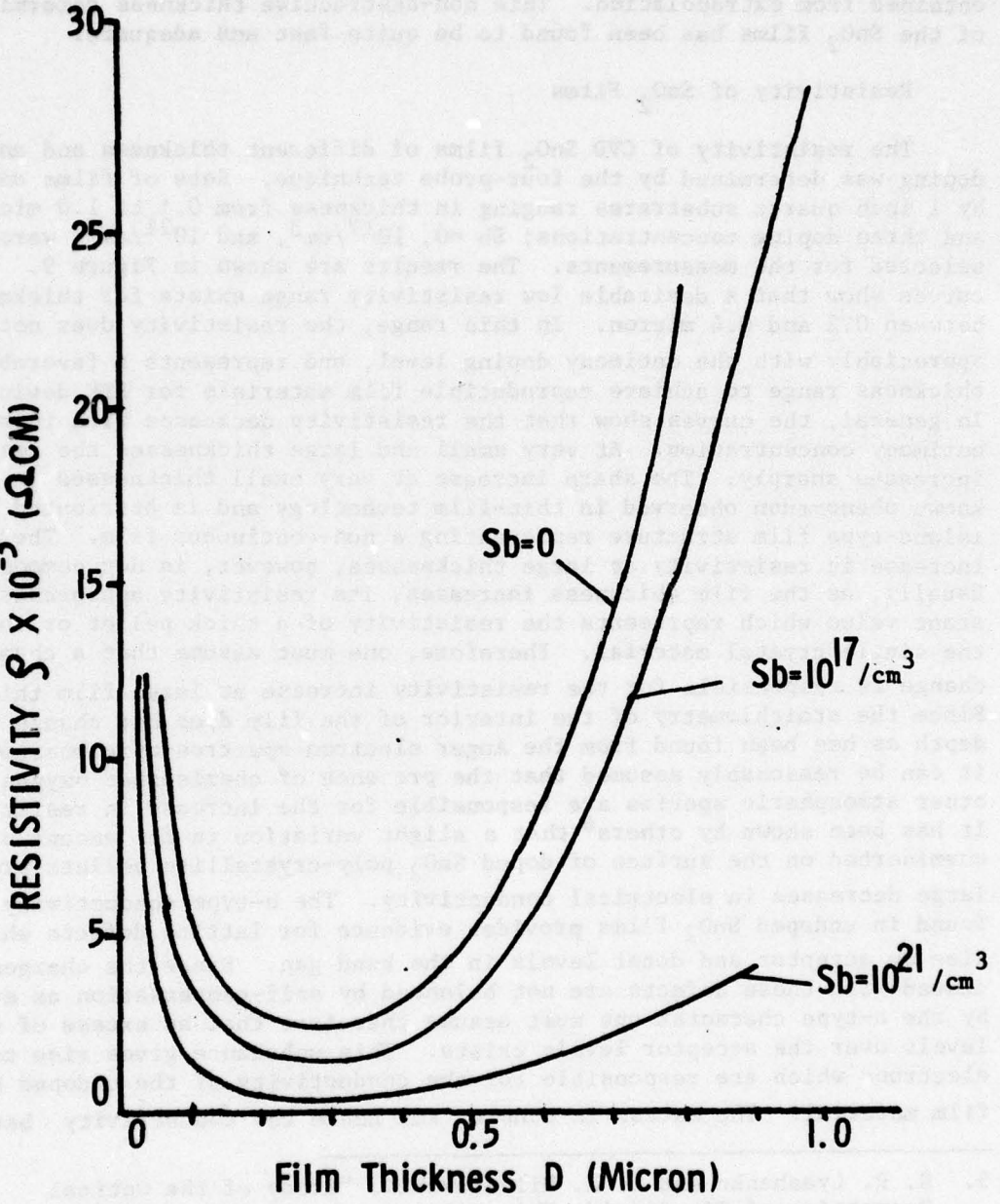

Figure 9. Resistivity of Sb-Doped SnO_2 - Films as a Function of Film Thickness

larger when SnO_2 films are intentionally doped, for example, with Sb^{3+} ions. Chemisorption of oxygen on the SnO_2 film leads to a substantial increase in the concentration of acceptor states of the surface which can immobilize the free electrons in the bulk. This reduces the concentration of the free electrons and in turn increase the resistivity of the film.

On the basis of the sharp increase in film resistivity at large thicknesses, it may be explained as follows: As the thickness of the undoped SnO_2 film increases during the chemical vapor deposition, the crystallites of the film grow larger. The lattice structure becomes more perfect and the number of free electrons decreases. This means that even a fraction of a monolayer of chemisorbed gases, such as oxygen, is now capable of trapping the free bulk electrons to a high degree. As a consequence of that, the resistivity of the film increases drastically, and continues to do so with increasing film thickness. The trapping of electrons by the chemisorbed gas layer leads to a film layer beneath the surface which has been depleted of electrons and so becomes a layer of high resistivity. The thickness of this depletion layer is proportional to the inverse of the density of the bulk electrons. Large differences between surface and bulk resistivity of undoped SnO_2 single crystals, for example, have been found with surface resistivities of several orders of magnitude higher, as compared to those of the bulk.[7]

The increase in resistivity with film thickness is less pronounced for the antimony SnO_2 films. Because of the much higher density of free electrons in the doped films as compared to the undoped film, the number of electrons required to neutralize a monolayer of chemisorbed oxygen or other atmospheric species (about $10^{14}/cm^2$) is relatively small. Therefore, one can assume, that the thickness of the depletion layer is relatively smaller than it is for the undoped film, and hence less sensitive to affect the film resistivity.

Temperature Dependence of Resistivity

The activation of SnO_2 film RTE elements, which will be discussed in detail later, involves the electrical heating of the film element by passing a current through it at increasing film voltages. In particular, the strongest heating occurs in the necked-down portion of the film element at which the emitter region is formed. One can reasonably assume that the temperature rise in this portion of the film will introduce notable changes in resistivity and probably also changes in the stoichiometry as to affect significantly the film current in the activation process of the RTE element. Therefore, it is important to study the temperature dependence of resistivity of CVD film samples.

The measurements were performed on undoped and antimony doped SnO_2 film samples on 1/2 x 1/2 inch quartz substrates. Metallization at both ends of the sample for electrical contact consisted of vacuum evaporated chromium strips with an overlay of gold to prevent oxidation. The film

---

7. J. A. Marley and R. C. Dokerty, "Electrical Properties of Stannic Oxide Single Crystals," Phys. Rev. 140, pp. A304, 1965.

sample was attached to a quartz sample holder with gold-plated tantalum pressure contacts with leads connecting to an ohmmeter. The film sample temperature was measured with a thermocouple attached to the sample holder. The holder with the sample was then placed in a quartz tube which was inserted into a high-temperature furnace, the temperature of which was programmed to a nearly linear rise. The film sample was heated in an inert atmosphere using a continuous flow of argon gas through the quartz tube. Film resistance and temperature were monitored continuously during the heating cycle with a two-pen strip recorder. Because the SnO_2 film samples were of different thicknesses but had equal areas, it was more appropriate to compare their resistivities rather than their resistance. The following relation was used for the conversion of resistance R to resistivity ρ :

$$\rho = C \times R \times d, \text{ where } C = \frac{W}{L}$$

and W and L are the width and length respectively of the film between contact strips, and d is the film thickness in centimeter.

The resistivity as a function of temperature for an undoped and for two antimony doped SnO_2 films is shown in Figure 10. The temperature dependence of resistivity of the three samples showed a minimum at 375°C which appeared to be more pronounced for the undoped SnO_2 film. Above 375°C, the resistivity increase exhibited two peaks at 475°C and just below 600°C. A third major peak in the resistivity above 600°C appeared to shift to higher temperature as the amount of doping in the films increased. Above 700°C all films showed a steep increase in resistivity which partially is due to evaporation (reducing film thickness) and probably partially due to loss in the pressure contact. In a separate experiment where a film was heated above 800°C, an appreciable thickness reduction due to evaporation was observed.

In the temperature range from room temperature (RT) to 600°C, film resistivity upon cooling was reversible. This indicated that in this temperature range the observed resistivity changes were controlled by the temperature coefficient of resistivity (TCR) of the SnO_2 film material. This TCR appeared to be negative in the range RT to 350°C, becoming zero and then positive above 350°C. The reversibility of the resistivity in the temperature range from RT to 600°C, also indicated that no compositional changes of the SnO_2 film had taken place. This was substantiated by X-ray diffraction data taken of a film doped with Sb = $10^{21}/cm^3$ after heating at 600°C. The diffraction pattern did not show any deviation from that of a SnO_2 pattern. Only a slight sharpening of the individual diffraction lines were observed, indicating recrystallization of the film particles.

Above 600°C the temperature dependence of resistivity was not reversible upon cooling, but increased strongly when the furnace was turned off and allowed to cool down to room temperature. This is shown in Figure 11, where the resistance of a Sb = $10^{21}/cm^3$ doped SnO_2 film is represented during the cooling cycle. The resistance at RT shows a ten-fold increase over that of its original value before heating. In a second experiment, Figure 12, a doped SnO_2 film (Sb = $10^{18}/cm^3$) was similarly heated to 650°C, and then cooled to RT. As before, the resistance had increased approximately by a factor of 10. After the cooling cycle, the film was heated a second time to 650°C during which the resistance was recorded. This time, a more pronounced minimum of the resistance curve at 350°C was observed.

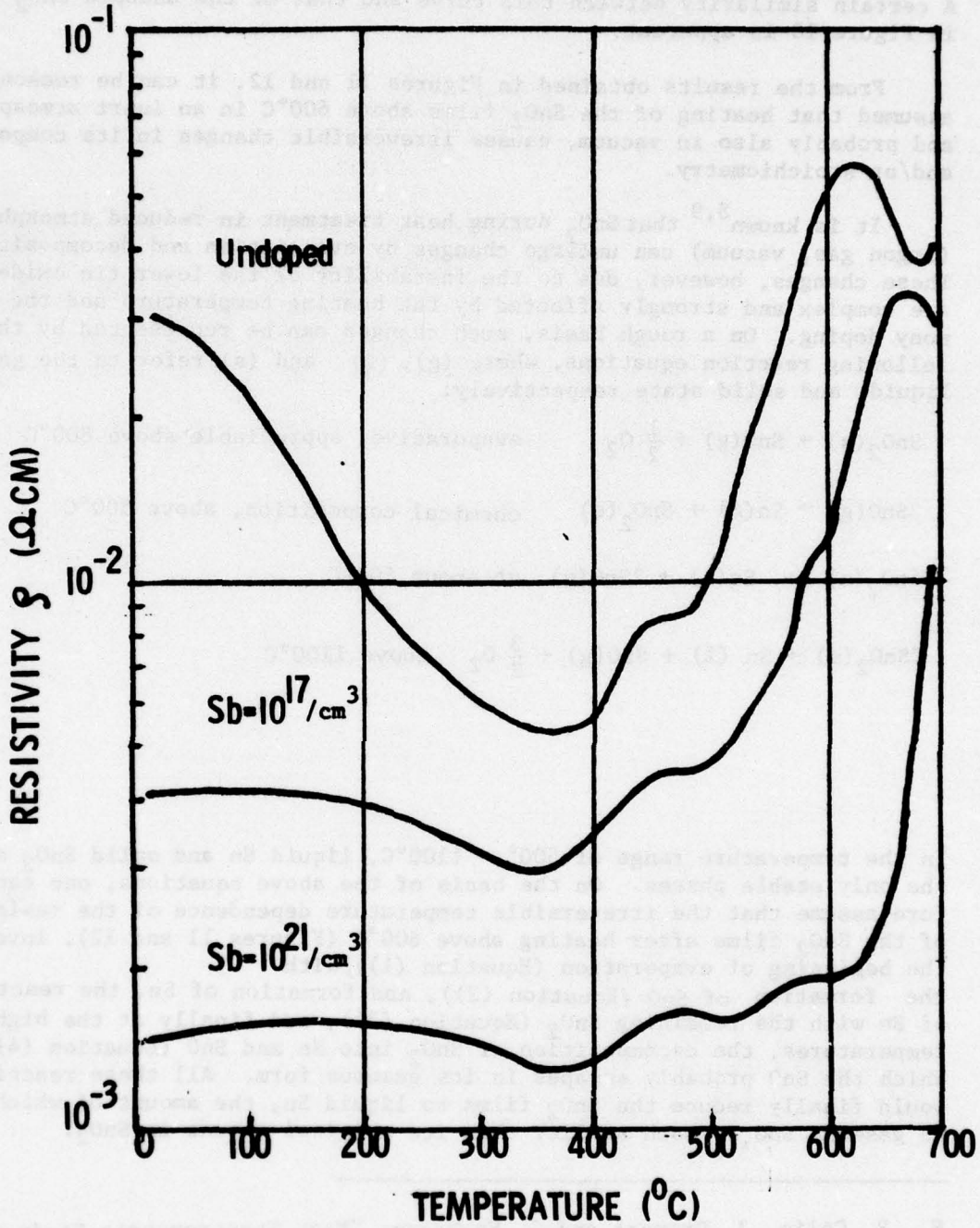

Figure 10. Resistivity of Undoped and Doped SnO_2 Films as a Function of Temperature

A certain similarity between this curve and that of the undoped SnO_2 film in Figure 10 is apparent.

From the results obtained in Figures 11 and 12, it can be reasonably assumed that heating of the SnO_2 films above 600°C in an inert atmosphere and probably also in vacuum, causes irreversible changes in its composition and/or stoichiometry.

It is known[8,9] that SnO_2 during heat treatment in reduced atmospheres (argon gas, vacuum) can undergo changes by evaporation and decomposition. These changes, however, due to the instability of the lower tin oxide, SnO, are complex and strongly affected by the heating temperature and the antimony doping. On a rough basis, such changes can be represented by the following reaction equations, where (g), (ℓ) and (s) refer to the gaseous, liquid, and solid state respectively:

$$SnO_2(s) \rightarrow SnO(g) + \frac{1}{2} O_2 \qquad \text{evaporative, appreciable above 800°C} \qquad (1)$$

$$2SnO(g) \rightarrow Sn(\ell) + SnO_2(s) \qquad \text{chemical composition, above 500°C} \qquad (2)$$

$$SnO_2(s) + Sn(\ell) \rightarrow 2SnO(g) \qquad \text{at about 600°C} \qquad (3)$$

$$2SnO_2(s) \rightarrow Sn\ (\ell) + SnO(g) + \frac{3}{2} O_2 \qquad \text{above 1100°C} \qquad (4)$$

In the temperature range of 500° - 1100°C, liquid Sn and solid SnO_2 are the only stable phases. On the basis of the above equations, one can therefore assume that the irreversible temperature dependence of the resistance of the SnO_2 films after heating above 600°C (Figures 11 and 12), involves the beginning of evaporation (Equation (1)), with the formation of SnO (Equation (2)), and formation of Sn, the reaction of Sn with the remaining SnO_2 (Equation (3)), and finally at the higher temperatures, the decomposition of SnO_2 into Sn and SnO (Equation (4)), by which the SnO probably escapes in its gaseous form. All these reactions would finally reduce the SnO_2 films to liquid Sn, the amount of which, due to gaseous SnO, is much smaller than its original amount in SnO_2.

---

8. R. Colin, J. Drowart and G. Verhagen, "Mass Spectrometric Study of the Vaporization of Tin Oxide," Trans. Faraday Soc. 61, pp. 1364, 1965.

9. J. C. Platteeuw and G. Meyer, "The System Tin-Oxygen," Trans. Faraday Soc. 52, pp. 1066, 1956.

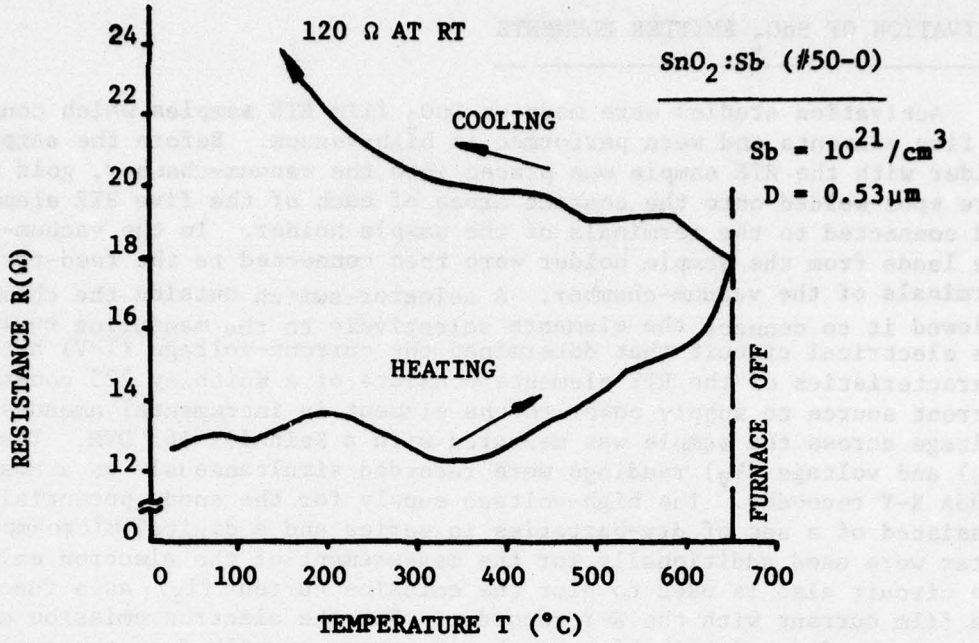

Figure 11. Resistance of a SnO_2:Sb Film During Heating and Cooling Cycle in Argon

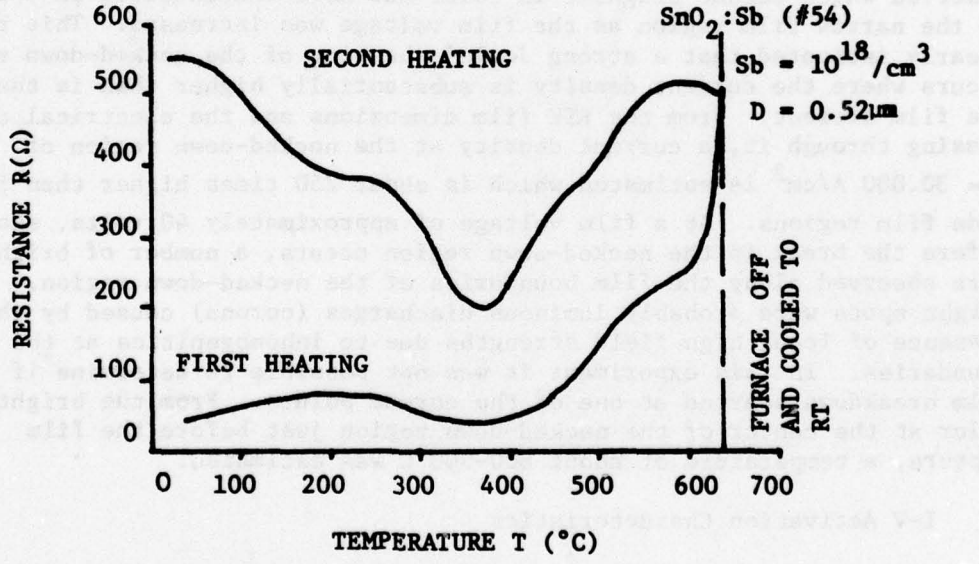

Figure 12. Resistance Vs.Temperature Characteristic of a SnO_2:Sb Film at the First and Second Heating

ACTIVATION OF SnO_2 EMITTER ELEMENTS

Activation studies were made on SnO_2 film RTE samples which consisted of five elements and were performed in high-vacuum. Before the sample holder with the RTE sample was placed into the vacuum-chamber, gold wires were spot-welded onto the contact areas of each of the five RTE elements and connected to the terminals of the sample holder. In the vacuum-chamber the leads from the sample holder were then connected to the feed-through terminals of the vacuum-chamber. A selector-switch outside the chamber allowed it to connect the elements selectively to the measuring equipment. The electrical circuit that determined the current-voltage (I-V) activation characteristics of the RTE elements consists of a Keithley 225 constant current source to supply power to the element in incremental amounts. The voltage across the sample was measured with a Keithley 163 DVM. The current (I_F) and voltage (V_V) readings were recorded simultaneously on a Mosely 7035A X-Y recorder. The high-voltage supply for the anode potential which consisted of a set of dry-batteries in series and a digital microampere meter were used additionally for the measurement of the electron emission. The circuit also is used to plot the emission current (I_E) as a function of the film current with the X-Y recorder. For the electron emission measurements an anode assembly which can be operated manually from the outside of the vacuum-chamber was placed in front of the RTE element. The distance of the anode from the RTE element was also adjustable from the outside.

An initial activation experiment was performed in air in order to observe the necked-down region of the RTE element under the microscope during the activation process. In this experiment the film voltage was increased stepwise. A red glow of the entire necked-down region was observed which became brighter in color and more concentrated in the center of the narrow film region as the film voltage was increased. This red glow clearly indicated that a strong Joule's heating of the necked-down region occurs where the current density is substantially higher than in the rest of the film element. From the RTE film dimensions and the electrical current passing through it, a current density at the necked-down region of $j = 30{,}000\ A/cm^2$ is estimated, which is about 250 times higher than in the wide film regions. At a film voltage of approximately 40 volts, shortly before the break in the necked-down region occurs, a number of bright spots were observed along the film boundaries of the necked-down region. These bright spots were probably luminous discharges (corona) caused by the presence of local high field strengths due to inhomogenities at the boundaries. In this experiment it was not possible to determine if the film breakdown started at one of the corona points. From the bright red color at the center of the necked-down region just before the film rupture, a temperature of about 800-900°C was estimated.

I-V Activation Characteristics

The actual activation experiments were performed in high-vacuum, as discussed above, the current through the RTE element caused strong heating of the necked-down region, until, at further increase of the voltage across the element, the film current suddenly broke down. The film current did

not vanish completely, but was reduced to an extremely small value, indicating that the necked-down region or part of it had changed from the original low-resistance state to a high-resistance state. In order to observe the effect of heating and subsequent changes of the RTE element during the activation process on the I-V characteristic, the X-Y recorder was used to continuously plot the film current (Y) at slowly increasing film voltages (X).

Two RTE arrays of different antimony doping and film thickness were used in the investigation. The I-V characteristics as plotted with X-Y recorder are shown in Figure 13. The left graph represents the I-V curves of three RTE elements of the array (RTE 49-0) doped with Sb = $10^{17}/cm^3$ and of film thickness D = 0.1 micron. The activation curves of the three elements were obtained at different rates of the film voltage (V_F) increase. Element No. 1 was activated in 10 minutes (4.7 volts/min), element No. 3 in 15 minutes (3.8 volts/min), and element No. 5 in 30 minutes (1.46 volts/min). All curves showed steplike structures which indicated deviations of the SnO_2 film material from a simple ohmic behavior. It can reasonably be assumed that these deviations are caused essentially by the extensively heated necked-down region of the film element.

The details in the I-V characteristics are more pronounced for the longer activation times. This can be explained by the longer time available for the necked-down region to assume equilibrium temperature at increasing film currents. Therefore, it can be assumed that the I-V curve obtained for a 30 minute activation time represents the curve for nearly equilibrium conditions. It was also observed that the maximum film current of the breakdown film voltage decreased as the activation time increased. No systematic dependence of the breakdown voltage on the activation time, however, was found. At these voltages the film current actually did not go to zero, but assumed a value of more than 1000 times smaller (too small to be observable in the plot) of that before the breakdown. After the activation, the RTE element exhibited a different type of I-V curve to which we refer to as the post-activation I-V characteristic. This characteristic will be discussed in more detail later in this section.

The initial slope of the I-V curves for the three elements (Figure 13), decreased slightly from element No. 1 to element No. 5. The resistances determined from these slopes are:

Element No. 1 - R = 1333 ohms

Element No. 2 - R = 1429 ohms

Element No. 3 - R = 1667 ohms

This spread in resistance indicates that the film elements do not have uniform thicknesses. Assuming equal geometry and doping concentration, the film thickness from element No. 1 to No. 5 decreases by 25 percent. Such deviations in film thickness has been frequently found across SnO_2 film samples prepared by the CVD method.

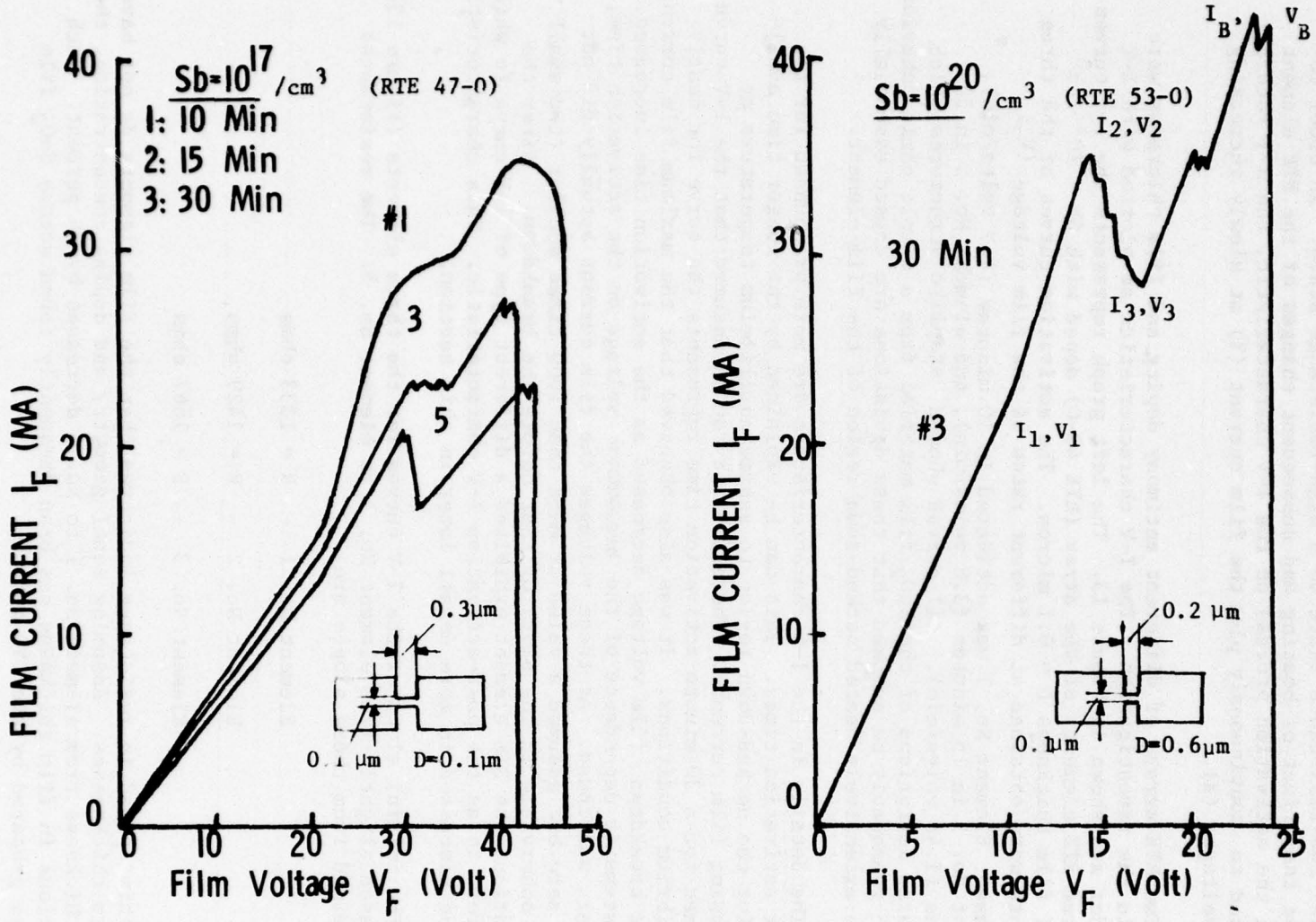

Figure 13. Activation Characteristics of Different Room Temperature Emitter Elements

At 20 volts the initial slope of the I-V curve increased, and at about 30 volts a constant current step occurred (elements No. 1 and 3) which reduced to a steep decrease in current as the activation time increased (element No. 5). This current break is probably corrected with a change in the temperature coefficient of resistance (TCR) of the heated necked-down region of the RTE element. The current voltage relationship in the 20-30 volt range of the activation curves indicates that the TCR changes from a negative to a zero and then to a positive value. A comparison of these current changes and subsequently resistance changes with the temperature dependence of the resistivity of SnO_2 films in Figure 10 shows a similar change in TCR at 350°C. This suggests that the necked-down region of the RTE element has attained this temperature at the applied film voltage of about 30 volts. Furthermore, one can speculate that at the film current breakdown at about 45 volts, the necked-down region has reached a temperature above 800°C which corresponds to the temperature at which the resistivity of the SnO_2 films in Figure 10 increase sharply. This temperature also agrees with the temperature value which was estimated from the microscopic observation of the necked-down region during the activation of an RTE element in air, described above.

The activation I-V characteristic of element No. 3 of an RTE array (RTE 53-0) with an antimony doping of Sb = $10^{20}/cm^3$ is shown on the right of Figure 13. The film thickness of this element, D = 0.6 micron, is larger than that of RTE 47-0. The width of the necked-down region is 0.2 millimeter which is less than that of the RTE 47-0 elements. The activation time was 30 minutes, the same as element No. 5 of RTE 47-0. One observes that the activation characteristics of both elements are very similar. The main differences, however, are the maximum current at the breakdown voltage which is somewhat higher for element No. 3 of RTE 53-0 and the much lower breakdown voltage of V_B = 24 Volts. Because of the higher dopant concentration, and larger film thickness, the initial resistance R = 444 ohms, is only one-third of that of element No. 5 of RTE 47-0.

The similarity of both I-V characteristics is more apparent by comparing corresponding points such as marked in the right graph of Figure 13 after normalizing their voltage and current values with respect to the breakdown voltage V_B and current I_B at the breakdown respectively. The results are shown in Table 1. The data show the close similarity between I-V activation characteristics of SnO_2 RTE elements of different doping levels, different film thicknesses, and different geometries of the necked-down region. It was also interesting to observe that the change in the initial slope of the I-V curve, at V_B, occurs at a voltage about one-half that of the breakdown voltage V_B, and the first major step occurred at about 2/3 of V_B.

Table 1

COMPARISON OF THE I-V CHARACTERISTICS OF ELEMENT NO. 5, RTE 47-0 AND ELEMENT NO. 3, RTE 53-0

RTE ELEMENT	V_1/V_B	V_2/V_B	V_3/V_B	I_1/I_B	I_2/I_B	I_3/I_B
No. 5, RTE 47-0 D = 0.1μm, Sb = $10^{17}/cm^3$	0.48	0.67	0.72	0.56	0.91	0.67
No. 3, RTE 53-0 D = 0.6μm, Sb = $10^{20}/cm^3$	0.46	0.63	0.70	0.54	0.88	0.69

Electron Microscopic Study of the Activated RTE Element

A series of activated SnO_2 RTE elements were inspected in the scanning electron microscope. Special emphasis was placed on the inspection of the necked-down region of the element. The micrographs revealed three major features which are schematically shown in Figure 14.

1. The formation of a filament across the center of the necked-down region.

2. A web-like structure protruding from the filament and extending far beyond the necked-down region.

3. The web-like structure always exists at the negative polarity side of the film element.

The electron micrograph showing these features is shown in Figure 15. It shows the necked-down region and part of the negative polarity side of the film element. The gray portion in the photograph represents the SnO_2 film while the dark portion shows the quartz substrate from which the SnO_2 film has been removed by photo-etching to form the necked-down region. The metal contacts, not seen, are located far out to the right and left side of the micrograph. The density of the web-like structure is quite dense close to the filament, and becomes less dense towards the negative contact area. It is believed that the filament represents a rupture of the film, and is formed at the moment when the current breakdown occurs during the

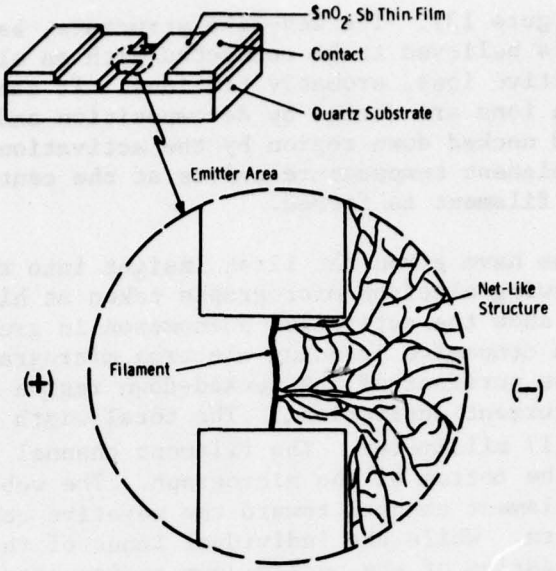

Figure 14. Activation Mechanism of the SnO_2 Room Temperature Emitter

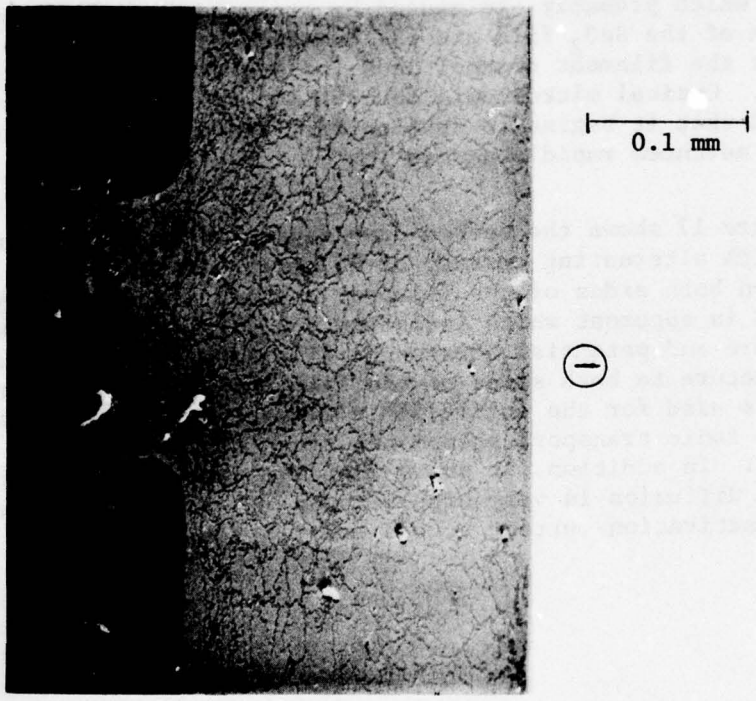

Figure 15. Scanning Electron Micrograph of the Activated Necked-Down SnO_2 Film Region of the RTE Element (X = 225)

activation process (Figure 13). The web-like structure, because of its polarity dependence, is believed to be connected with an electric field supported flow of positive ions, probably tin ions. It can be reasonably assumed that these tin ions are formed by decomposition and/or evaporation of the strongly heated necked-down region by the activation current. It is believed that the highest temperature exists at the center of the necked-down region where the filament is formed.

These observations have given the first insight into the activation mechanisms. The following electron micrographs taken at higher magnifications will serve to show the activation phenomenon in greater detail. Figure 16 represents a composite scanning electron micrograph taken in sequence of consecutive portions of the necked-down region of an RTE element after direct current activation. The total width of the necked-down region is W = 0.17 millimeter. The filament channel formed across this neck is seen at the bottom of the micrograph. The web-like structure protruding from the filament channel toward the negative contact seems to follow a complex pattern. While the individual lines of this structure close to the film boundaries of the necked-down region seem to follow current flux lines, they are nearly parallel to the filament of some distance away from it. This indicates that a potential gradient also existed across the necked-down region which probably is caused by the incomplete rupture of the films, along the filament channel and by the non-uniformity of its width. The film boundaries of the neck region show rupture-like irregularities which probably are caused by stress due to differences in thermal expansion of the SnO_2 film and the quartz substrate. It is interesting to note that the filament channel ends (or starts) at one of these irregularities. Optical microscopic observation of the formation of the filament indicated that it begins to develop from one side of the necked-down region and then advances rapidly across it.

Figure 17 shows the necked-down region of an RTE element after activation with alternating current of 60 hertz. Here the web-like structure appears on both sides of the filament channel. A certain symmetry of this structure is apparent which indicates a highly symmetrical distribution of temperature and potential across the filaments. The appearance of the web-like structure to both sides of the filament channel when an alternating current is used for the activation element, strongly supports our hypothesis about the ionic transport phenomenon along the lines of the web-like structure. In addition, it shows that the rate of the electrical field supported diffusion is very high because the polarity change for the 60 hertz activation current occurs every 8.3 milliseconds.

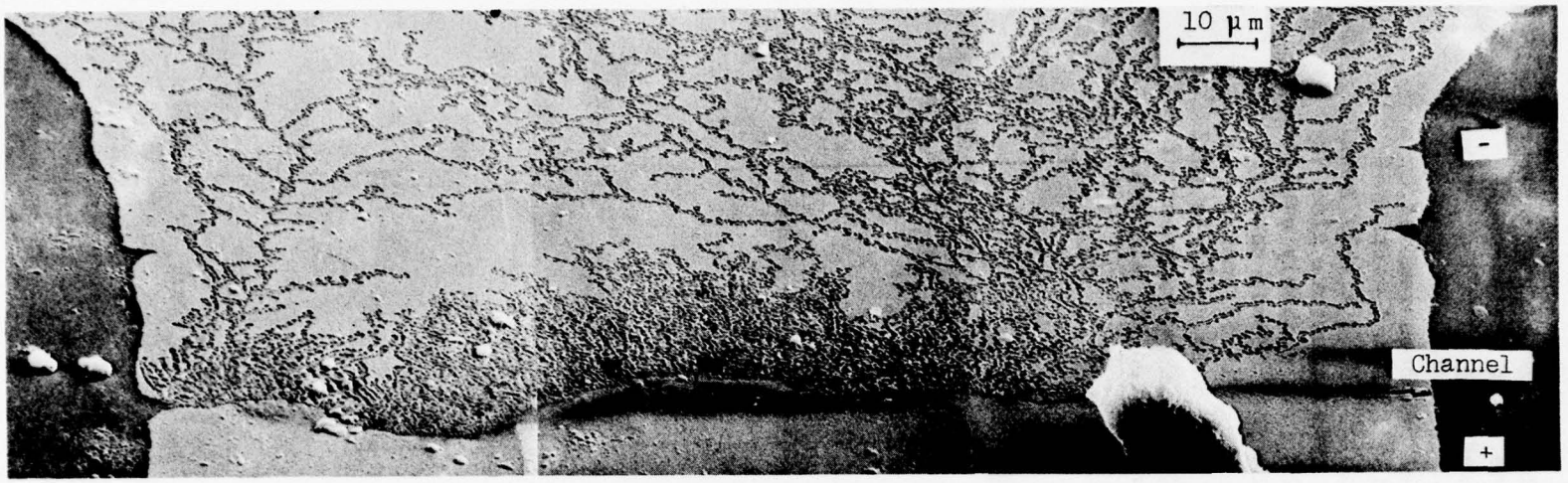

Figure 16. Electron Micrograph of the Necked-Down Film Region After dc Activation (X = 1122)

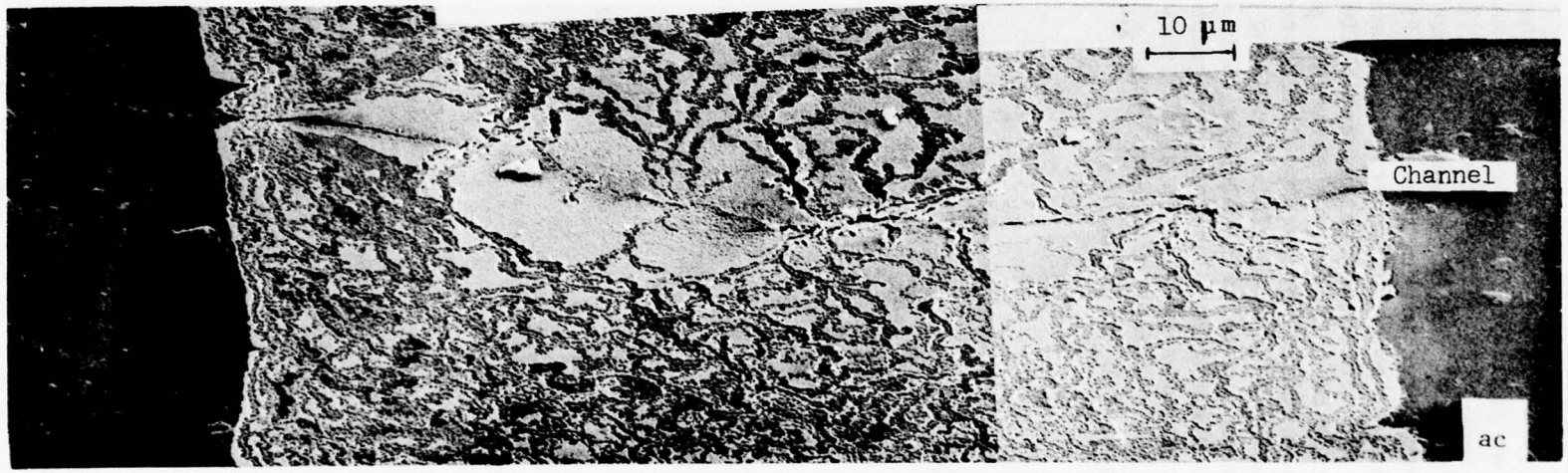

Figure 17. Electron Micrograph of the Necked-Down Film Region After ac Activation (X = 1152

Figure 18 shows two typical terminations of the filament channel in the necked-down region at about twice the magnification as in the previous figure. Again, the portion above the filament corresponds to the negative polarity side of the RTE element. These scanning electron micrographs clearly show that within the channel film material has been removed by a melting and/or evaporation process, leaving occasional island portions of it in the center of the channel. Similarly, Figure 19, a highly magnified section of the web-like structure shows that this structure also is formed by a melting or decomposition process in the film probably caused by the diffusion of the metallic tin along rain-boundaries. These channels however, seem not to be completely "burned-out" as the main filament. In Figure 20 a scanning electron micrograph taken at a 0° viewing angle (all other micrographs were taken at 60° viewing angle) allows measurement of the width of the filament channel. In this specific activated RTE element, the width was about 1000Å.

Figure A. X = 2367

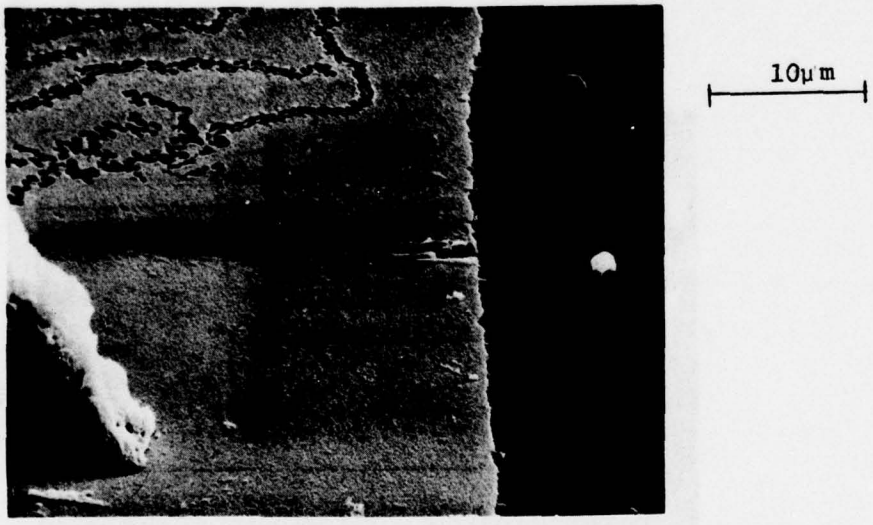

Figure B. X = 2320

Figure 18. Scanning Electron Micrographs of Two Typical Channel (Filament) Terminations at the Necked-Down Region of the SnO_2 RTE Element

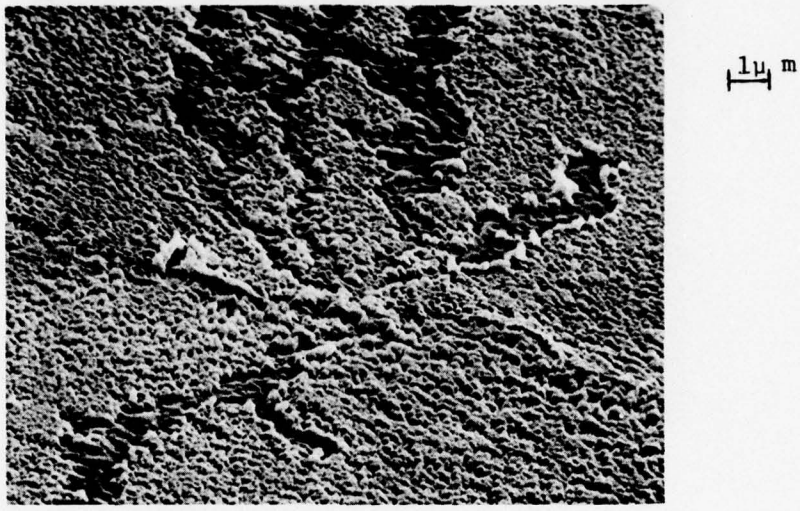

Figure 19. Scanning Electron Micrograph of a Portion of the Web-Like Structure under Higher Magnification (X = 5830)

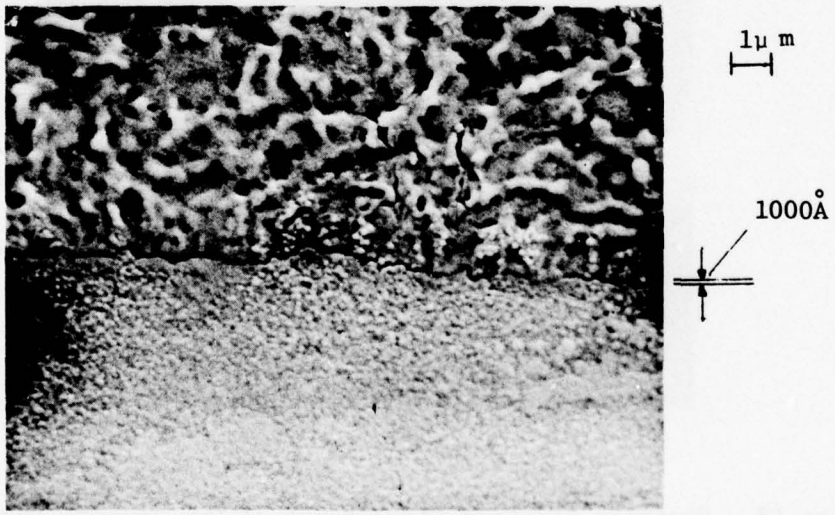

Figure 20. High Magnification Scanning Electron Micrograph of the Channel at Perpendicular Viewing of the Activated SnO_2 Film Surface (X = 5822)

AUGER ELECTRON SPECTROSCOPY OF THE ACTIVATED RTE ELEMENT

Surface Auger electron spectroscopy is applied to obtain information about the chemical nature of the web-like structure. For this purpose, the primary electron beam focussed to a diameter of about 100 micron is directed onto three different positions of an activated RTE element. These positions are selected at the positive polarity site of the element, the center of the necked-down region, and at the negative polarity side of the element where the web-like structure is present. Portions of the spectra obtained from the three selected positions covering the tin and oxygen Auger signals are shown in Figure 21 togther with the diagram of the RTE element, and the positions at which the Auger spectra were taken.

The spectra obtained at positions A and B show about equal strength of the corresponding tin (Sn) and oxygen (O) peaks. The spectrum for position C, however, shows the tin peak being absent and the oxygen peak being considerably smaller than at positions A and B. At higher Auger electron energies - not shown here - the three spectra also have a small silicon (Si) peak (at 1619 eV) which is strongest for position C. The peak-to-peak amplitudes (in mm) measured at the original chart recordings of the tin, oxygen and silicon Auger signals for the three positions of the RTE element are given in Table 2.

Table 2

COMPARISON OF THE AUGER SIGNALS

Auger Signal	Position Across RTE Element		
	A	B	C
Sn	113	107	0
O	118	110	74
Si	7	10	17

A reasonable explanation for the absence of the tin Auger signal at position C is that the channels of the web-like structure represent areas at which the SnO_2 film material has been removed in the activation process. Furthermore, because of the high density of these channels, the remaining SnO_2 film area between the channels is too small to allow detection of its tin Auger signal.

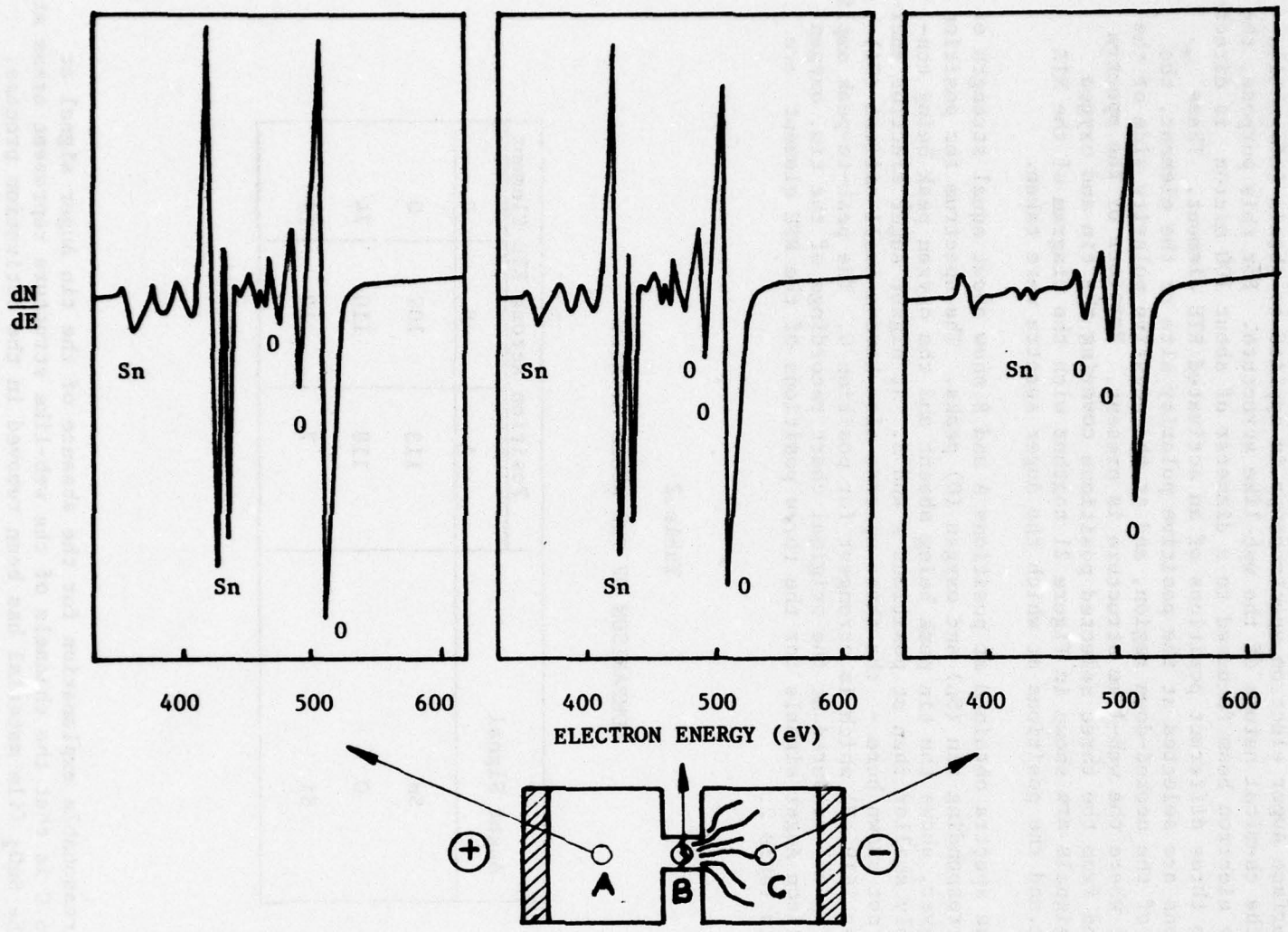

Figure 21. Auger Electron Spectrograms of an Activated SnO_2 RTE Element at Three Different Positions as Indicated.

If we assume that the sampled depth in Auger spectroscopy is in the order of 10 Å and that the area analyzed is determined by the diameter of the resident electron beam probe which is 100 micron, the analyzed volume is then 8×10^{-12} cm^3. If we further assume that 1 cm^3 of SnO_2 contains 10^{22} tin atoms, the analyzed volume then contains 8×10^{10} tin atoms. Since the Auger signal is proportional to the number of atoms of the species of interest in the analyzed volume, the 8×10^{10} tin atoms are equivalent to a peak-to-peak amplitude of 113 mm as found for position A (See Table 2). Because the amplitude of the noise level in the recorded Auger spectrum is about 1 mm, the detection limit for tin would be $8 \times 10^{10}/113 \approx 7 \times 10^8$ atoms. From this, it follows that the tin concentration at position C must be smaller at least by a factor of 100 as compared with the tin concentration at position A where no web-like structure exists.

The presence of an appreciable oxygen Auger signal at position C in spite of the undetectable tin probably originates from the exposed quartz substrate within the channels of the web-like structure where the SnO_2 film material has been removed. This is supported by the existence of a fairly strong silicon Auger signal (Table 2).

The values for the Auger signals at position B appear to be rather high. This might be explained by the difficulty in aligning the primary electron beam precisely at the center of the necked-down region. The measured values indicate that the incident beam has been probably positioned more towards the A position of the element.

In order to substantiate these Auger spectroscopic results, specifically those obtained for position C, the micro-probe analysis method has been applied. The results obtained confirmed the Auger data, namely that no tin was found within the channels of the web-like structure. The micro-probe data, however, revealed a somewhat higher tin concentration at the channel boundaries as compared to the tin concentration in the remaining SnO_2 film material between the channels.

From the results of the scanning electron microscopic observation, the Auger spectroscopy, and the micro-probe analysis, we conclude that the SnO_2 film material within the channels of the web-like structure has been removed by thermal decomposition. It can reasonably be assumed that the web-like structure develops along grain-boundaries as shown schematically in Figure 22. The figure shows the main filament across the necked-down film region of the RTE element. It is believed that during its formation, high concentrations of tin have been deposited at the wall of the filament. The development of the individual channels of the web-like structure which protrudes from the wall of the main filament are controlled by the diffusion of tin metal along the grain-boundaries towards the negative polarity side of the device.

A grain-boundary is an agglomeration of vacancies, interstitials and other imperfections. Diffusion of atomic species along such grain-boundaries is much faster than volume diffusion through the grains itself. The already lower resistivity of grain-boundaries as compared with that of the grains is further reduced by the diffusion of tin. As a consequence of that, the post-activation film current is preferentially distributed along

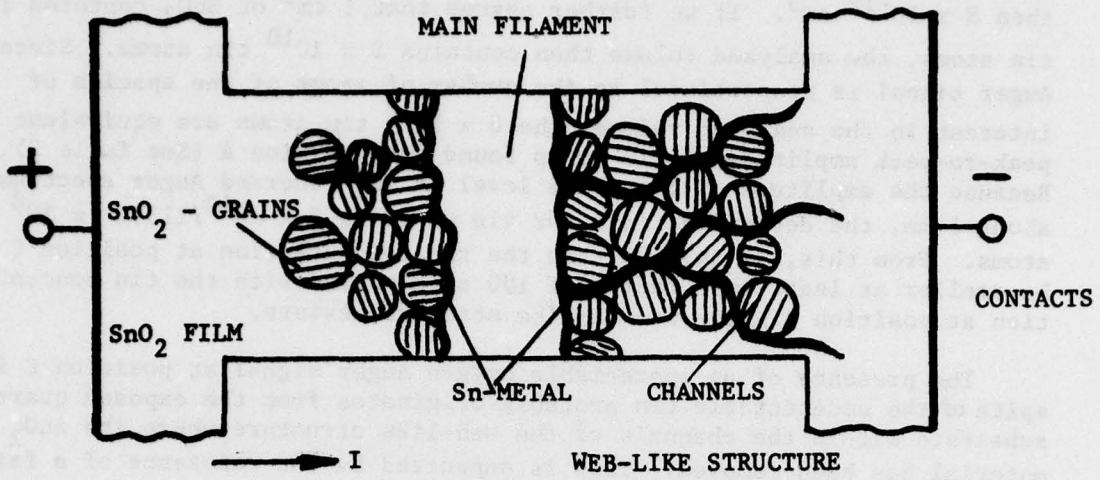

Figure 22. Schematic Representation of the Proposed Formation of the Web-Like Structure.

the grain-boundaries where high current densities can be expected to exist. These high current densities are sufficient to cause locally a strong heating with the result that the material along the grain-boundary melts and decomposes and in this way forms the channels of the web-like structure. In this forming process, molten tin remains, which, in part solidifies on the wall of the channel and conducts the film current. The tin metal diffuses further along the grain-boundary, and participates in the continuation of the channel formation process.

In a separate investigation the kinetics of the formation of channels was observed in the optical microscope while an RTE element was activated in air. It was observed that the main filament across the necked-down film region forms instantly when the film current breakdown occurs. The web-like structure protruding from the main filament, however, slowly advances toward the negative polarity side when the breakdown voltage across the RTE element is maintained. In another RTE element which was activated in the same way, the film voltage, however, was turned to zero immediately after the activation. In this case, no web-like structure evolved from the filament. If the film voltage, however, is slowly increased again from zero, channels start to protrude and grow with increasing voltages. These results strongly support the above proposed mechanism of the formation of the web-like structure as part of the activation process of SnO_2 film RTE elements.

POST-ACTIVATION I-V CHARACTERISTIC AND SEASONING EFFECT

As discussed earlier, the RTE element when activated, changes to a high resistance state. In this state the film current is about 1000 times smaller and the I-V curve character is different from that of the I-V curve exhibited before the activation. With regard to this post-activation I-V characteristic, the following observations have been made:

1. Tracing the I-V curve at increasing film voltages, the film current appears very erratic. Tracing the curve, however, repeatedly at increasing and decreasing voltages, the post-activated I-V curve stabilizes. The erratic behavior of the film current probably is due to the development of the web-like structure with increasing voltages as discussed in the previous section.

2. Reversing the polarity of the film voltage after stabilization of the post-activation I-V curve, the film current assumes significant higher values. Microscopic inspection reveals that the web-like structure now appears at the opposite side of the main filament (now being the negative polarity side). This is in agreement with the electron microscopic observation (Figure 17) of the web-like structure appearance when ac voltage is applied to activate the RTE element. The appearance of the web-like structure in the opposite side of the filament with subsequent increase in film current, indicates strongly that the presence of web-like structure lowers the resistance of the corresponding film portion of the RTE element. This reduction in resistance is probably due to the highly conductive channels of the web-like structure.

3. Seasoning of an activated RTE element with or without applied voltage for hours or days increases the film current and hence results in

a steeper post-activation I-V characteristic.

Figure 23 shows a series of post-activation I-V curves traced before and after seasoning for 100 hours. The lower set of curves is obtained before seasoning. Here, the solid curve is traced with the film voltage's polarity being the same as it has been when the element was activated (forward bias). The dashed curve represents the I-V curve if the film voltage polarity is reversed (reversed bias). As can be seen, reversing the polarity of the film voltage results in a somewhat higher film current. The upper set of curves represents the corresponding I-V curves after seasoning the activated RTE element for 100 hours. After the seasoning, the film current has increased by nearly a factor of 50.

The I-V curve in the high resistance state of the activated RTE element shows a non-ohmic behavior. The current obeys the relationship $I = V^n$ with $n = 2$. A non-ohmic behavior is a characteristic feature of semiconductors either at high temperature or at high electrical field. In both cases this can be interpreted as ionization of defect centers. Because of the high current density in the channels of the web-like structure and because of the heating effect connected with it, we believe that thermal ionization in the SnO_2 film sections adjacent to the channels is responsible for the non-ohmic behavior.

Figure 24 shows the details of the seasoning experiment. The freshly activated RTE element was kept for 120 hours in the high-vacuum chamber. During this period the film current at 20 volts applied in the forward direction was recorded at certain intervals. In order to see if the seasoning is affected when voltage is applied continuously, the film voltage was kept across the RTE element for periods of time. The seasoning periods without and with applied voltages are indicated in the graph. It can be seen that a much faster rate of the current increase can be obtained during the seasoning period if a voltage to the RTE element is applied. While the rate of current increase without applied voltage is only about 1 μA/hour, the rate with applied voltage is about 30 μA/hour, i.e., approximately 30 times faster. Therefore, seasoning with applied voltage can significantly reduce the seasoning period.

The seasoning characteristic also shows that there exists a limit for the current increase by the seasoning. This is indicated by the current maximum at about 100 hours. One observes that in the interval of 92-100 hours with the voltage applied, the rate of current increase starts to level off. Continuation of the seasoning without applied voltage leads to a sharp decrease of the current. Further seasoning with the voltage applied again appears to restore this current decrease.

Seasoning of the activated RTE element was also observed with reversed polarity of the applied voltage. While the film current is much higher, as discussed above, the rate of current increase due to seasoning, however, is about the same as that when the voltage is applied to the forward direction.

The results of the seasoning experiment can be interpreted also in terms of a diffusion mechanism, similar to that involving the formation of

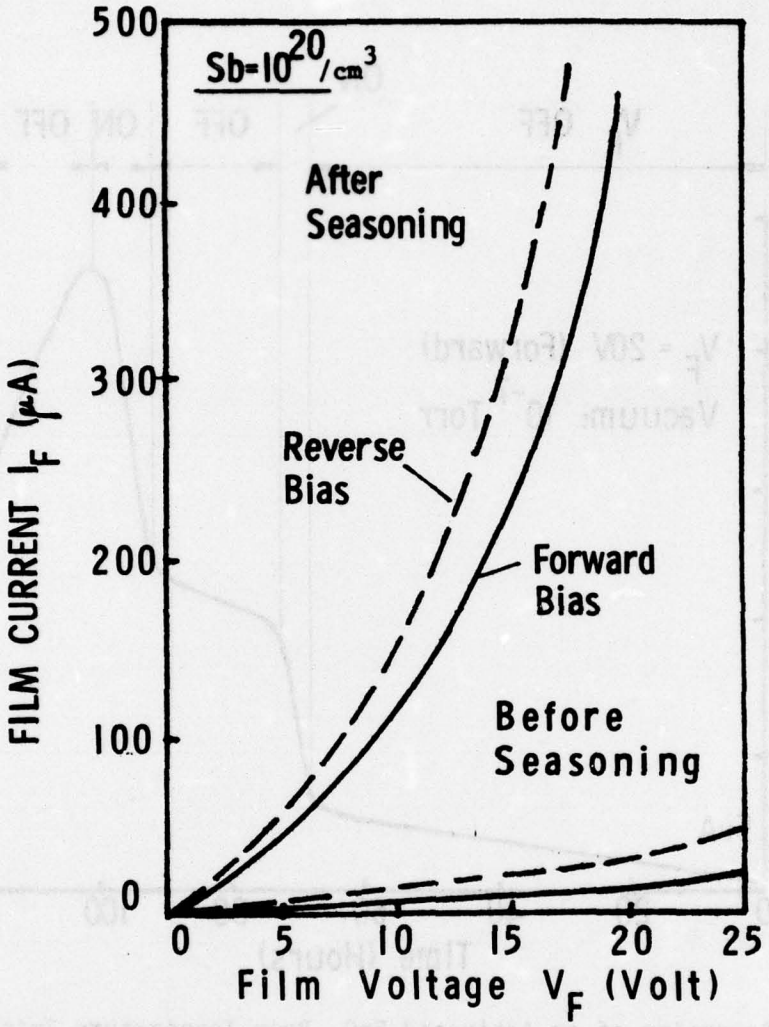

Figure 23. Post-Activation I-V Characteristic of the SnO_2 Room Temperature Emitter (RTE 53-0, #3.) The Effects of Film Voltage Polarity and Seasoning are also shown.

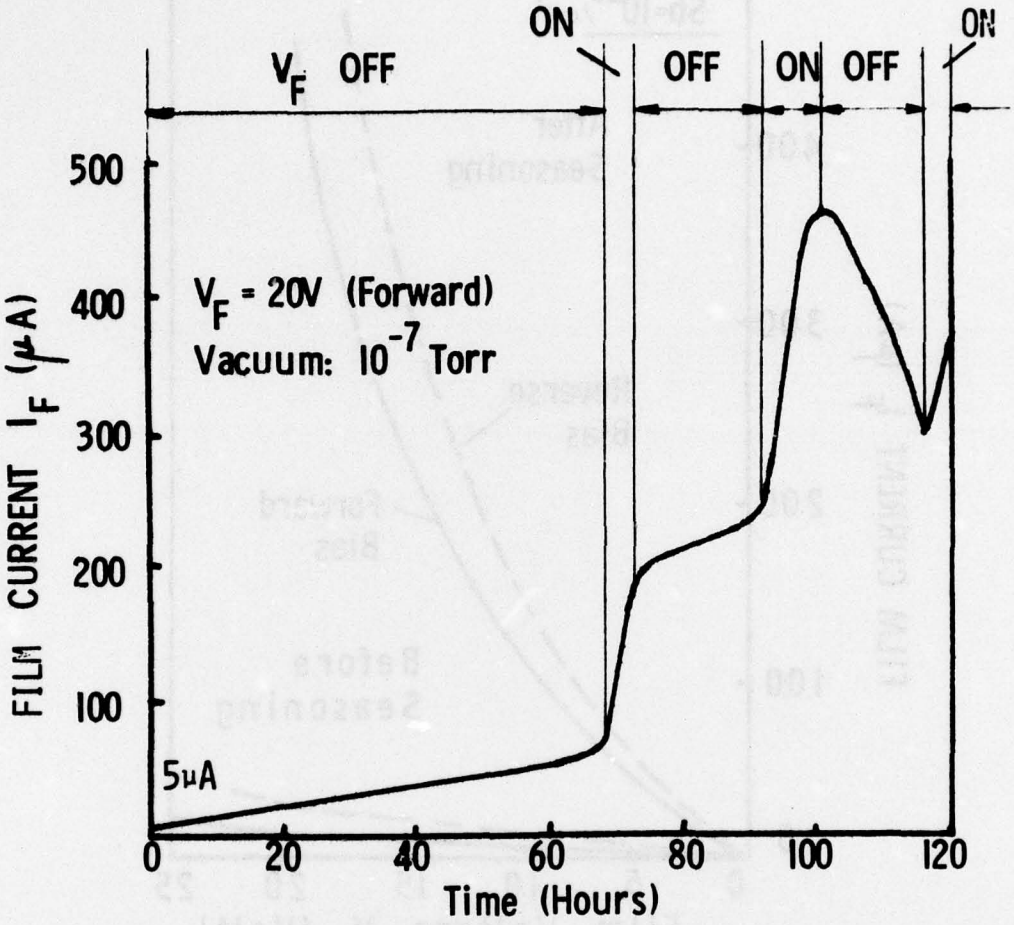

Figure 24. Seasoning of an Activated SnO_2 Room Temperature Emitter Element (RTE 53-0, #3) Intermittent Without and With Applied Film Voltage.

the channels of the web-like structure. In the latter case, the driving force for the diffusion of tin along grain boundaries is furnished by the gradient in temperature and by the force of the electrical field (thermally and field induced). The driving force for diffusion of tin in the seasoning mechanism is furnished by the concentration gradient only if no voltage is applied, and by the concentration gradient and the electrical field if a voltage is applied during the seasoning. From the rate of current increase in both cases it is evident that the electrical field supported diffusion rate is about 30 times higher than the diffusion rate supported by the concentration gradient without applied voltage.

ELECTRON EMISSION OF THE SnO_2 RTE

Element No. 2 of the RTE array 47-0, doped with $10^{17}/cm^3$ antimony was activated and used for the room-temperature electron emission measurements. The anode distances from the RTE element was adjusted to 1 millimeter. The anode voltage selected was V_A = 900 volts. Two X-Y recorders were applied to record concurrently, both the post-activation current, and the electron emission current as a function of film voltage V_F. The measurements were performed when V_F was applied to the forward and the reversed direction.

Figure 25 shows the results which are typical of the SnO_2 RTE. The solid curves represent the film current, the dashed curves the emission current. The lower set of these curves was obtained for film voltages applied in the forward direction. The upper set of curves represent the corresponding currents for film voltages applied to the reversed direction.

It can be seen that, except for high emission currents which indicate a saturation effect, the electron emission is nearly proportional to the film current. Using the ratio of emission and film current $\eta = I_E/I_F$ as criterion for the electron emission efficiency, it can be shown that η is about 30 percent for the forward direction of the film voltage, and slightly higher, about 40 percent for the reversed direction of the film voltage.

The precise mechanism of the electron emission of the SnO_2 RTE is not well understood. The results obtained, however, indicated that the main filament across the necked-down region of the element which was formed in the activation process, is the origin of the emission. Micro-probe measurements of the potential distribution across the activated RTE element showed that large electrical fields can be expected at the main filament region. As discussed previously, the width of this filament was found to be about 1000Å. Applying a film voltage of V_F =100 volt and assuming that the major potential drop occurs across the filament, the electric field strength would be in the order of $E = 10^7$ V/cm which is sufficient to support field emission. Figure 26 shows schematically the potential distribution to be expected along the RTE element. The potential distribution is shown when the film voltage is applied first in the forward direction and subsequently applied in the reversed direction. In the

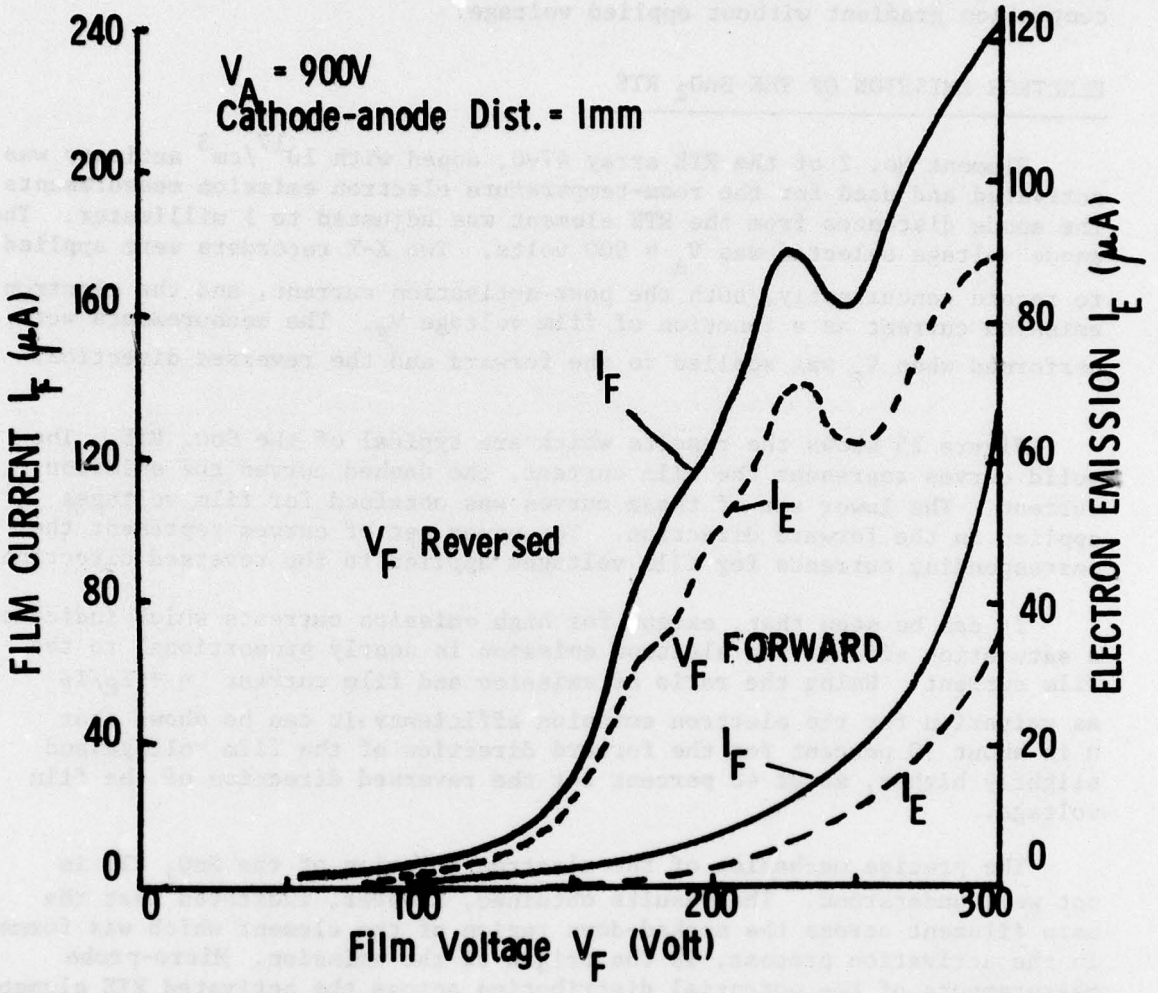

Figure 25. Post-Activation I-V Characteristic and Electron Emission Current of the SnO_2 RTE No. 47-0, Element No. 2.

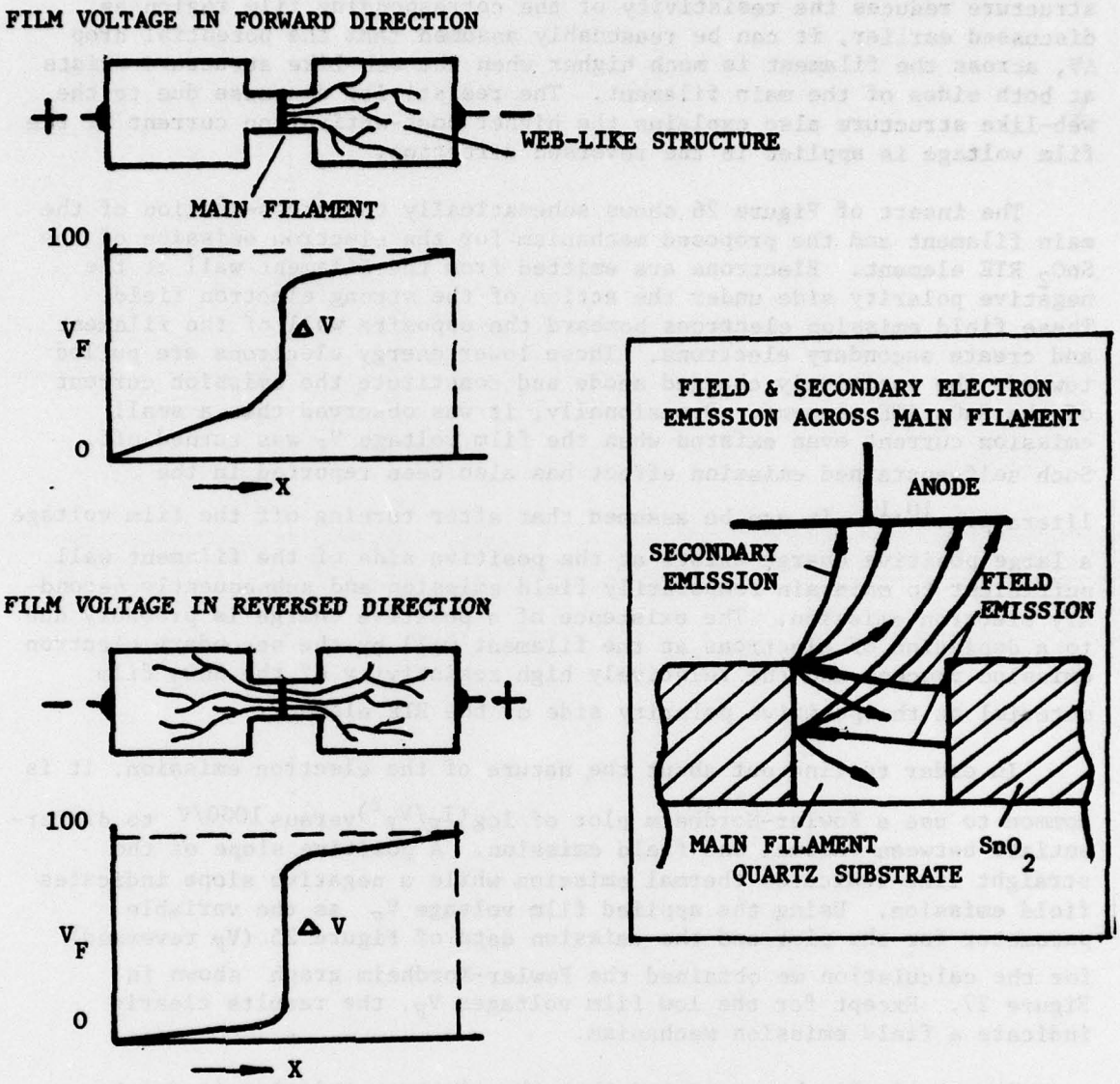

Figure 26. Potential Distribution Along the Activated RTE Element with Film Voltages Applied in the Forward and in the Reversed Direction. Insert: Proposed Field and Secondary Electron Emission Mechanism.

first case, the web-like structure develops from the filament towards the negative polarity side, in the second case a similar structure protrudes from the opposite of the filament. Since the presence of the web-like structure reduces the resistivity of the corresponding film region as discussed earlier, it can be reasonably assumed that the potential drop ΔV, across the filament is much higher when the web-like structure exists at both sides of the main filament. The resistivity decrease due to the web-like structure also explains the higher post-activation current if the film voltage is applied in the reversed direction.

The insert of Figure 26 shows schematically the cross-section of the main filament and the proposed mechanism for the electron emission of the SnO_2 RTE element. Electrons are emitted from the filament wall at the negative polarity side under the action of the strong electron field. These field emission electrons bombard the opposite wall of the filament and create secondary electrons. These lower energy electrons are pulled towards the positively charged anode and constitute the emission current of the SnO_2 RTE element. Occasionally, it was observed that a small emission current even existed when the film voltage V_F was turned off. Such self-sustained emission effect has also been reported in the literature.[10,11] It can be assumed that after turning off the film voltage a large positive charge exists at the positive side of the filament wall sufficient to maintain temporarily field emission and subsequently secondary electron emission. The existence of a positive charge is probably due to a depletion of electrons at the filament wall by the secondary electron emission process and the relatively high resistivity of the SnO_2 film material at the positive polarity side of the RTE element.

In order to find out about the nature of the electron emission, it is common to use a Fowler-Nordheim plot of $\log(I_E/V_F^2)$ versus $1000/V$ to differentiate between thermal and field emission. A positive slope of the straight line indicates thermal emission while a negative slope indicates field emission. Using the applied film voltage V_F as the variable parameter for the plot and the emission data of Figure 25 (V_F reversed) for the calculation we obtained the Fowler-Nordheim graph shown in Figure 27. Except for the low film voltages V_F, the results clearly indicate a field emission mechanism.

Because it has been assumed that the electron emission is due to secondary electrons, the Fowler-Nordheim field emission characteristic is explained by a close proportionality between the primary electron emission current I_P and the secondary electron emission current I_E.

---

10. T. A. Raju and B. J. Harrell, "Manifestations of Sustained Secondary Electron Emission from Tin Oxide Films," J. Appl. Phys. 40, pp. 4213, 1969.

11. Takao Hanasaka, Toru Satake, Masao Hashiba and Teshiro Yamashina, "Electron Emission From Vacuum Evaporated Tin-Oxide Films," Japan, J. App. Phys. Suppl. 2, Part 1, pp. 227, 1974.

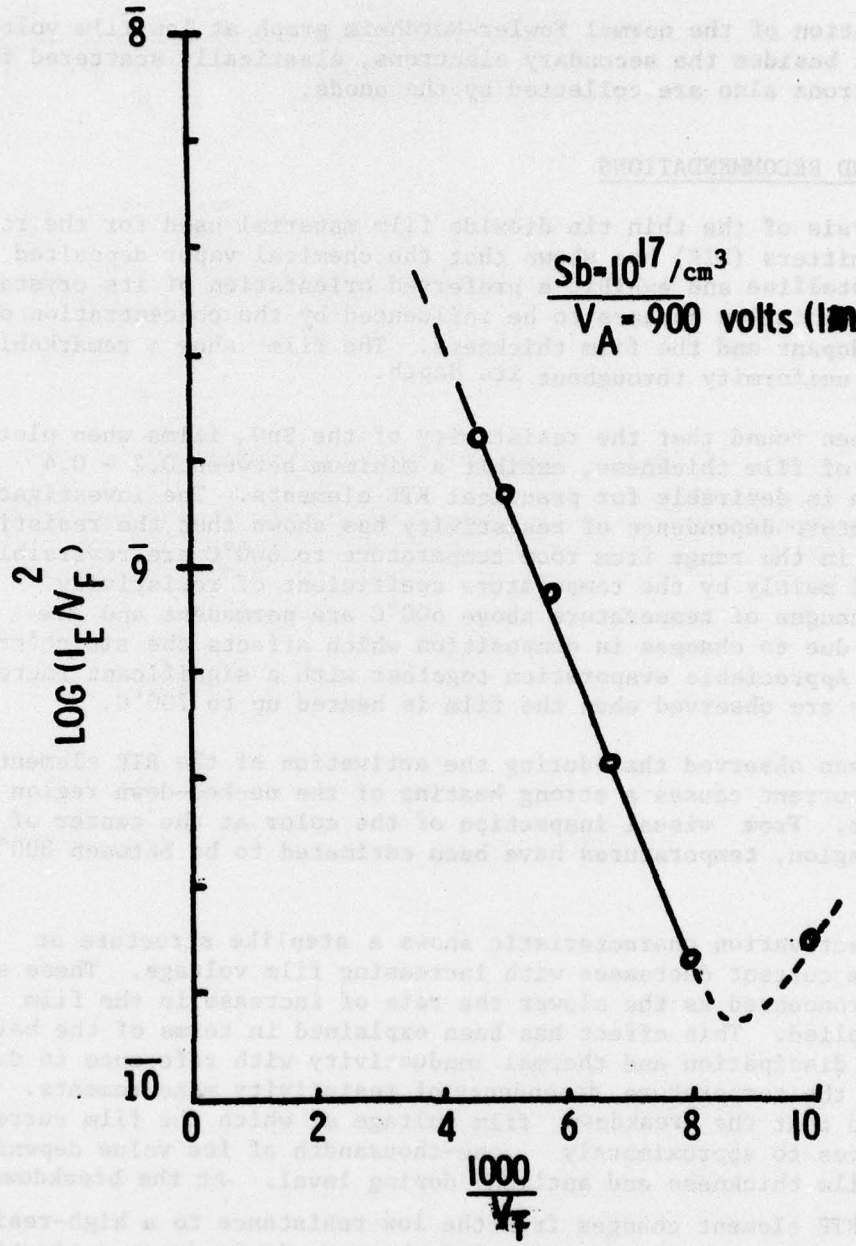

Figure 27. Fowler-Nordheim Plot of the Dependence of Emitter Current on Film Voltage (RTE 47-0, No. 2).

It is known[12] that the secondary emission ratio $\delta = {}^{I_E}/_{I_p}$ for low primary electron energies is nearly proportional to V_p. This probably explains the typical field emission characteristic of the Fowler-Nordheim graph.

The deviation of the normal Fowler-Nordheim graph at low film voltages indicates that besides the secondary electrons, elastically scattered field emission electrons also are collected by the anode.

CONCLUSIONS AND RECOMMENDATIONS

The analysis of the thin tin dioxide film material used for the room temperature emitters (RTE) has shown that the chemical vapor deposited films are crystalline and exhibit a preferred orientation of its crystallites. The orientation appears to be influenced by the concentration of the antimony dopant and the film thickness. The film show a remarkable compositional uniformity throughout its depth.

It has been found that the resistivity of the SnO_2 films when plotted as a function of film thickness, exhibit a minimum between 0.2 - 0.4 micron, which is desirable for practical RTE elements. The investigation of the temperature dependence of resistivity has shown that the resistivity variation in the range from room temperature to 600°C are reversible and controlled mainly by the temperature coefficient of resistivity. Resistivity changes of temperature above 600°C are permanent and are assumed to be due to changes in composition which affects the stoichiometry of the SnO_2. Appreciable evaporation together with a significant increase in resistivity are observed when the film is heated up to 700°C.

It has been observed that during the activation of the RTE elements the electric current causes a strong heating of the necked-down region of the element. From visual inspection of the color at the center of the necked-down region, temperatures have been estimated to be between 800° and 900°C.

The I-V activation characteristic shows a steplike structure at which the film current decreases with increasing film voltage. These steps become more pronounced as the slower the rate of increase in the film voltage is applied. This effect has been explained in terms of the balance between power dissipation and thermal conductivity with reference to data obtained from the temperature dependency of resistivity measurements. It has been found that the breakdown film voltage at which the film current suddenly reduces to approximately one-thousandth of its value depends on the SnO_2 film thickness and antimony doping level. At the breakdown voltage, the RTE element changes from the low-resistance to a high-resistance state and exhibits an activation I-V characteristic (post-activation characteristic) which is different from that of the low-resistance state.

---

12. H. Bruining, Die Sekundar-Elektronen Emission Fester Körper, Verlag Julius Springer, Berlin, 1942, Edward Brothers Inc., Ann Arbor, Mich., Chapter III and IV, 1944.

It has been demonstrated that in reversing the polarity (reversed direction) of the film voltage, significant higher film currents can be obtained.

Inspection of the activated area in the necked-down region of the RTE element in the scanning electron microscope has revealed the formation of a filament across the center of the necked-down film region. The presence of a web-like channel structure which protrudes from the filament is always toward the negative polarity side of the element. When using alternating current (ac) for the activation, the web-like structure appears symmetrically to both sides of the filament. The filament has been identified as a rupture in the film, about 1000Å wide. Furthermore, it has been established that the web-like structure develops after the formation of the filament, and growth is visible as the film voltage is increased. Its formation has been explained in terms of an electric field supported tin diffusion along grain-boundaries, and locally increased current densities. As a consequence of this, thermal decomposition of the SnO_2 material along the diffusion path occurs. The tin metal which remains causes a reduction of the total resistivity of the web-like structure region.

It has been demonstrated that seasoning of the activated RTE element, with or without applied voltage results in an increase in the film current. The electron emission of the activated element is nearly proportional to the film current, and is higher when the film voltage is reversed. It has been proposed that the electron emission is mainly a secondary electron emission generated by a field emission mechanism across the narrow main filament. This was substantiated by the construction of the Fowler-Nordheim plot, using the emission current and the film voltage as variables.

The results obtained in this study have provided a better understanding of the mechanisms of activation and emission of the SnO_2 room temperature emitter. It is felt that the performance of the device can be improved by further studies of the effect of the element geometry on the electrical and thermal conductivities, by exploring other methods of SnO_2 film preparation; for example, by sputtering, by improving the etching techniques in forming the RTE element and array geometries, and by selecting better electrical contact materials to the SnO_2 film in order to reduce the contact resistance.

It is believed that SnO_2 may not be the only material suitable for RTE. Recently, it has been demonstrated by others that tin doped indium oxide shows good potentiality as room temperature emitter material. If secondary electron emission, as proposed in this study, is the basic mechanics for the RTE device, it can reasonably be assumed that materials which possess good secondary electron emission capability together with low conductivity would be most advantageous as RTE material.

Preliminary experiments undertaken during this study with a focussed laser beam to activate the necked-down region of RTE elements have been encouraging. In addition, the laser beam activation method would also provide a possibility to obtain large emitter areas by scanning over large film areas either in a straight, circular, or other modes.

ACKNOWLEDGMENTS

The authors wish to thank Mr. C. Cook, Jr., for providing the electron diffraction patterns of the film materials, and the scanning electron micrographs of the activated RTE elments, Mr. D. Eckart for providing the X-ray diffractometer data of the SnO_2 films, Dr. K. Schwidtal and Mr. D. Fox for performing the Auger electron spectrographic measurements, all from the Electronic Materials Research Division, US Army Electronics Technology & Devices Laboratory, ERADCOM. Furthermore, the authors wish to thank Mr. Guy DeLhery for measuring the film thicknesses, Dr. J. O'Connell for determining the resistivities of the films by the four-probe technique, and Mrs. C. MacNeill for performing the high temperature resistivity measurements, all from the Beam, Plasma, and Display Division, US Army Electronics Technology & Devices Laboratory, ERADCOM.

REFERENCES

1. M. I. Elinson, A. G. Zhdan, G. A. Kudintseva and M. E. Chugunova, "The Emission of Hot Electrons and the Field Emission of Electrons from Tin Oxide," Rad. Eng. Elec. Phys. 8, pp. 1290, 1965.

2. V. V. Nikulov, G. A. Kudintseva, M. I. Yelinson, and L. A. Konsul Nikova, "The Emission Properties of Cold Cathodes Employing Tin Dioxide (SnO_2) Films," Rad. Eng. Elec. Phys. 17, pp. 1153, 1971.

3. J. L. Mize, "Investigation of Solid State Cold Cathodes," Final Report, Beta Industries, Inc., Contract No. DAAK-72-C-0163, 1972.

4. H. F. Kunkle and E. F. Kohnke, "Flux Growth of Stannic Oxide Crystals," J. Appl. Phys. 36, pp. 1489, 1965.

5. S. P. Lyashenko and V. K. Hiloslavskii, "Study of the Optical Properties of Tin Dioxide Thin Films in the Visible and Ultra-Violet Regions," Opt. and Spectr. 19, pp. 55, 1965.

6. H. E. Matthews and E. E. Kohnke, "Effect of Chemisorbed Oxygen on the Electrical Conductivity of Zn-Doped Polycrystalline SnO_2," J. Phys. Chem. Solids, 29, pp. 653, 1968.

7. J. A. Marley and R. C. Dokerty, "Electrical Properties of Stannic Oxide Single Crystals," Phys. Rev. 140, pp. A304, 1965.

8. R. Colin, J. Drowart and G. Verhagen, "Mass Spectrometric Study of the Vaporization of Tin Oxide," Trans. Faraday Soc. 61, pp. 1364, 1965.

9. J. C. Platteeuw and G. Meyer, "The System Tin-Oxygen," Trans. Faraday Soc. 52, pp. 1066, 1956.

10. T. A. Raju and B. J. Harrell, "Manifestations of Sustained Secondary Electron Emission from Tin Oxide Films," J. Appl. Phys. 40, pp. 4213, 1969.

11. Takao Hanasaka, Toru Satake, Masao Hashiba and Teshiro Yamashina, "Electron Emission From Vacuum Evaporated Tin-Oxide Films," Japan, J. App. Phys. Suppl. 2, Part 1, pp. 227, 1974.

12. H. Bruining, Die Sekundar-Elektronen Emission Fester Körper, Verlag Julius Springer, Berlin, 1942, Edward Brothers Inc., Ann Arbor, Mich., Chapter III and IV, 1944.

DEPARTMENT OF THE ARMY
HEADQUARTERS R&D
UNITED STATES ARMY ELECTRONICS COMMAND
FORT MONMOUTH, NEW JERSEY 07703
ATTN DRSEL-MS-TI
OFFICIAL BUSINESS

POSTAGE AND FEES PAID
DEPARTMENT OF THE ARMY
DOD-314